THE JOURNAL OF PHYSICAL CHEMISTRY B

Article

pubs.acs.org/JPCB

Fifth-Order Three-Dimensional Electronic Spectroscopy Using a Pump−Probe Configuration

Zhengyang Zhang, Kym L. Wells, Marco T. Seidel, and Howe-Siang Tan*

Division of Chemistry and Biological Chemistry, School of Physical and Mathematical Sciences, Nanyang Technological University, 21 Nanyang Link, Singapore 637371

Supporting Information

ABSTRACT: We present the theoretical details and experimental demonstration of fifth-order three-dimensional (3D) electronic spectroscopy using a pump−probe beam geometry. This is achieved using a pulse shaper and appropriate phase cycling schemes. We show how 8-step and 27-step phase cycling schemes can measure purely absorptive 3D spectra as well as 3D spectra for the individual fifth-order processes that contribute to the purely absorptive spectrum. 3D spectra as a function of two separate controllable waiting time periods can be obtained. The peak shapes and positions of the peaks in the experimental measurement correspond well to theory.

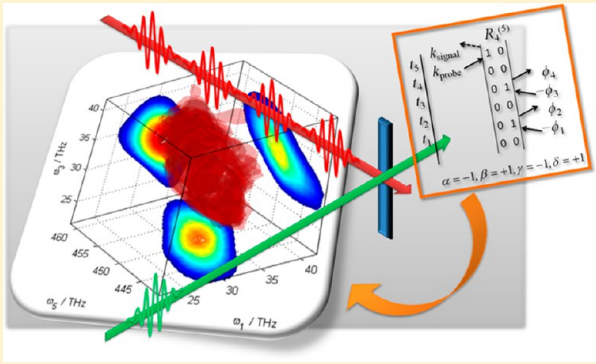

I. INTRODUCTION

The extension of the by now well-established two-dimensional (2D) third-order optical spectroscopies[1−6] to three-dimensional (3D) fifth-order optical spectroscopies[7−9] brings several new observables to the spectroscopist inaccessible in lower-order spectroscopies. This includes the ability to reach higher vibronic states to better characterize the anharmonicity of the investigated systems.[7,10−12] 3D spectroscopy also allows higher spectral resolution and declutters congested spectra, by introducing a third frequency axis.[12] In 3D electronic spectroscopy, one can retrieve hidden couplings that were previously obscured in a congested 2D electronic spectrum.[8] 2D electronic spectroscopy has been applied to studying energy transfers between excitonic states in light-harvesting complexes.[13] These processes are highly complicated and consist of multiple steps. 2D electronic spectroscopy can only directly observe single step energy transfers and indirectly infer multiple step energy transfer.[14] 3D electronic spectroscopy has the potential to provide direct measurements of multiple step energy transfer between these multilevel electronic systems. A recent topic of debate is the validity of commonly made assumptions, such as linear response theory, Gaussian statistics, and Markovian processes. As shown, 3D spectroscopies can help answer these questions by studying the three-point correlation function.[15,16] Recent work on liquid water unequivocally showed its heterogeneous structural relaxation dynamics.[9] From these examples alone, it is clear that fifth-order 3D spectroscopy will be of benefit for the optical spectroscopist and the extension to higher dimensions is expected to become even more pertinent with further advances in ultrafast laser technologies.

Figure 1a shows the fundamental idea of fifth-order 3D optical spectroscopy. The three coherence time periods t_1, t_3, and t_5 are Fourier transformed to measure the instantaneous frequencies ω_1, ω_3, and ω_5, respectively, at waiting times t_2 and t_4. Third-order 3D optical experiments have also been performed recently[17−19] where an extra frequency dimension can be obtained from a conventional third-order 2D optical spectroscopy experiment by Fourier transforming over the waiting time period. Unlike third-order 3D spectroscopy, which arises from three interactions with the light field, fifth-order 3D spectroscopy requires five interactions with the incoming light field. Fifth-order 3D spectroscopy in its conventional phase-matching implementation requires in its most general case six individual pulses (including a local oscillator pulse).[7] The intricate optical setup hampers the applicability of 3D spectroscopy, even more so than 2D spectroscopy.

A limited form of fifth-order 3D spectroscopy can be performed using only four pulses (including the local oscillator), as shown in Zanni's work in the infrared[12] and Engel's work in the visible,[8] where multiple interactions are made by the second and third pulses, to measure the fifth-order signal. This necessarily means that there is no control over the population times t_2 and t_4, which will always be equal to zero. The other limitations of using two interactions each for pulses one and three in Zanni's work or pulses two and three in Engel's work to achieve five interactions is that purely absorptive peaks cannot be obtained. A full form of fifth-order 3D spectroscopy with control over the population times was performed in the IR using a non-collinear phase-matching geometry with six pulses

Special Issue: Michael D. Fayer Festschrift

Received: May 10, 2013
Revised: June 28, 2013
Published: June 28, 2013

   dx.doi.org/10.1021/jp4046403 | J. Phys. Chem. B 2013, 117, 15369−15385

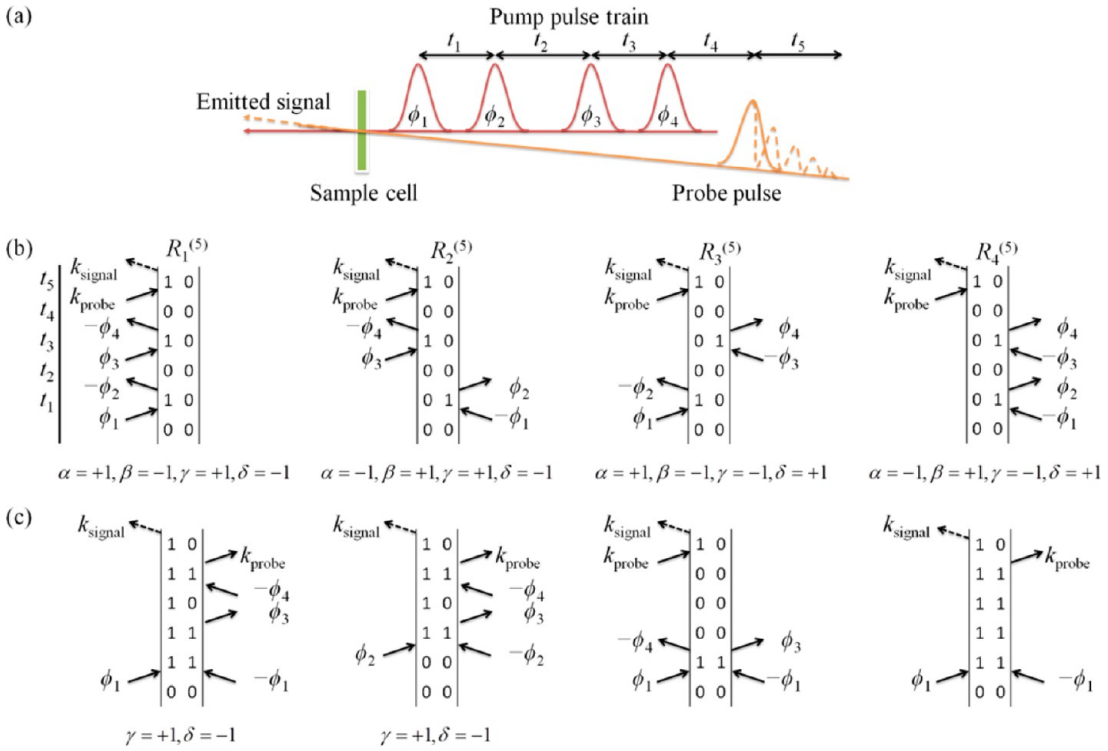

Figure 1. (a) Schematic setup for fifth-order 3D optical spectroscopy in a pump−probe geometry. The coherence times t_1 and t_3, the waiting time t_2, as well as the phases ϕ_1, ϕ_2, ϕ_3, and ϕ_4 are set by a pulse shaping apparatus, while the second waiting time t_4 is introduced by a delay stage. (b) Double-sided Feynman diagrams (DSFD) for fifth-order 3D spectroscopy on a two-level system in a pump−probe geometry contributing to the desired three-dimensional spectrum with populations during the waiting times. The resulting $\mathbf{k}_{signal}$ vector as well as the acquired phase ϕ_{signal} and phase signatures are denoted. (c) A brief selection of the multitude of DSDFs for undesired processes that can be eliminated by phase cycling. From left to right, these are pump−probe processes where the first pulse interacts twice, the second pulse interacts twice, or both pulses interact twice. Lower-order processes such as those shown on the far right need to be discriminated as well. Their acquired phase and phase signature are denoted where applicable.

(including the local oscillator) independently controlled using computer-controlled mechanical translational stages.[7] With the advent of 2D spectroscopy performed in a pulse shaper assisted pump−probe configuration, the experimental technique is simplified.[20−24] One further major advantage of such a pulse shaper assisted setup is that it allows the immediate extension to three dimensions and higher orders without the need of altering the optical setup. Recently, our group demonstrated a method to obtain purely absorptive fifth-order 3D electronic spectra based on a pulse shaper assisted pump−probe beam geometry setup.[25] In our 3D spectroscopy performed using a pump−probe configuration, the first four "pump" pulses are provided collinearly by a pulse shaper, followed by subsequent interaction by a non-collinear probe pulse. In principal, the advantages of 2D spectroscopy in a pump−probe geometry apply to 3D spectroscopy as well, such as intrinsic phasing of various contributions to the overall response function and data collection in the rotating frame, which allows under-sampling.[22,23,26,27] However, just like in the two-dimensional case,[23,27−30] to obtain three-dimensional spectra devoid of peak ambiguities and interferences from other spurious signals, phase cycling is essential. With phase cycling, the desired multidimensional signals can be retrieved by the weighted summation of data collected from using different interpulse phases. Phase cycling can be easily implemented using a pulse shaper by systematically changing the relative interpulse phases, which is cycled over 2π radians in a number of equally spaced steps.[27,28] Recent works have shown that, with the proper understanding of phase cycling theory and phase cycling scheme selection, two-dimensional spectra of desired Liouville pathways, such as rephasing and non-rephasing diagrams can be obtained.[21−23] In this article, the concept of phase cycling is extended to apply to the various implementations of 3D optical spectroscopy in the pump−probe beam geometry. The next section describes a general theoretical framework to choose appropriate phase cycling procedures needed to obtain fifth-order 3D spectra. Section III presents the experimental procedures for phase cycling in 3D spectroscopy, while in section IV, we report our results that are obtained from various phase cycling schemes. Section V outlines the possibility of cascaded third-order signals in the 3D spectrum from a pump−probe geometry setup. The publication summarizes with a brief conclusion in section VI.

II. THEORY

In the framework of diagrammatic time dependent perturbation theory, three-dimensional optical spectroscopy is a fifth-order nonlinear optical experiment where the system interacts five times with the incident light fields. Specifically, in the pump−probe beam geometry, the pump pulse light field interacts four times, while the fifth interaction is provided by the probe pulse. Phase matching conditions result in the induced fifth-order sample polarization, creating a signal light field that is emitted collinearly with the probe pulse, so that it is self-heterodyne detected and thus rendering an external local oscillator unnecessary. Since six light fields participate in the light−matter interaction, it is also referred to as a six-wave mixing process (SWM).

dx.doi.org/10.1021/jp4046403 | J. Phys. Chem. B 2013, 117, 15369−15385

A general scheme of a pump−probe geometry 3D optical experiment is shown in Figure 1a. The required phase-locked four pulse pump train can be readily provided by a pulse shaping apparatus,[31] with individually controllable coherence times t_1 and t_3, and waiting time t_2. Due to the limited temporal window of pulse shapers, there is a constraint on the achievable waiting time t_2, but this constraint may not be crucial in many cases. For instance, Hamm showed that, to study the three-point frequency fluctuation correlation functions, waiting times up to 3 ps are sufficient.[15] Such time delays pose no problem to current pulse shaping technology. All four pump pulses are incident along the wave vector $\mathbf{k}_{pump}$ and have the individual phases ϕ_1, ϕ_2, ϕ_3, and ϕ_4, respectively. The probe pulse is delayed by a second waiting time t_4 from the last pump pulse interaction via a translation stage and is incident onto the sample in the $\mathbf{k}_{probe}$ direction. The signal is emitted with the time delay t_5. Phase matching conditions make sure that the desired signal field is emitted along the direction of the probe pulse $\mathbf{k}_{probe} = \mathbf{k}_{signal}$, so that the probe pulse intrinsically acts as a local oscillator to self-heterodyne the signal field. We do not take into consideration the phase relationship between the pump and probe pulses, as they interact non-collinearly.[15] In section II.A, we will discuss the phase cycling schemes for such four pump pulse experiments.

As there has been growing interest to use the rephasing and non-rephasing spectra to observe energy transfers within light-harvesting complexes in 2D spectroscopy,[14,32,33] several groups have previously proposed ways to retrieve signals from the rephasing and non-rephasing processes in a pump−probe beam geometry setup.[21,23] Similarly, we can independently retrieve signals from the four different pathways that contribute to the pure absorptive 3D spectrum in a pump−probe beam geometry setup, which we will discuss in section II.B.

A. Purely Absorptive 3D Spectra Using Four Pump Pulses in a Pump−Probe Geometry. The pulse train incident on the sample in a 3D pump−probe experiment in a pump−probe geometry can be expressed in the time domain as

$$\begin{aligned} E(t) = {} & E_1(t + t_4 + t_3 + t_2 + t_1)\exp(-i\omega_L t + i\phi_1 + i\Delta\omega_{ref} t_1 + i\mathbf{k}_{pump} r) \\ & + E_2(t + t_4 + t_3 + t_2)\exp(-i\omega_L t + i\phi_2 + i\Delta\omega_{ref} t_2 + i\mathbf{k}_{pump} r) \\ & + E_3(t + t_4 + t_3)\exp(-i\omega_L t + i\phi_3 + i\Delta\omega_{ref} t_3 + i\mathbf{k}_{pump} r) \\ & + E_4(t + t_4)\exp(-i\omega_L t + i\phi_4 + i\mathbf{k}_{pump} r) \\ & + E_5(t)\exp(-i\omega_L t + i\mathbf{k}_{probe} r) + \text{c.c.} \end{aligned} \quad (1)$$

where E_1−E_5 denote the individual pulse envelopes and ω_L is the pulse center frequency, while $\Delta\omega_{ref}$ is the difference between the pulse center frequency ω_L and a reference frequency ω_{ref} set by the pulse shaper. In a "rotating frame", $\Delta\omega_L = \omega_L - \omega_{ref} = 0$.[22,23] The macroscopic signal field $S(t_1, t_2, t_3, t_4, t_5)$ is a convolution of the fifth-order nonlinear response function $R^{(5)}(t_1, t_2, t_3, t_4, t_5)$, which contains all relevant information about the system under investigation, and the interacting light fields:

$$\begin{aligned} S(t_1, t_2, t_3, t_4, t_5) = {} & \int\int\int\int\int dt_5\, dt_4\, dt_3\, dt_2\, dt_1 \\ & \times R^{(5)}(t_1, t_2, t_3, t_4, t_5) E(\mathbf{k}, t - t_5) E(\mathbf{k}, t - t_5 - t_4) \\ & \times E(\mathbf{k}, t - t_5 - t_4 - t_3) E(\mathbf{k}, t - t_5 - t_4 - t_3 - t_2) \\ & \times E(\mathbf{k}, t - t_5 - t_4 - t_3 - t_2 - t_1) \end{aligned} \quad (2)$$

In the semi-impulsive limit, i.e., when the pulse envelopes are considered as δ-functions while still retaining their carrier frequencies, phases, and wave vectors, the emitted light field is directly proportional to the response function.[6]

The fifth-order nonlinear response function $R^{(5)}(t_1, t_2, t_3, t_4, t_5)$ consists of various coherence transfer pathways which can be illustrated using double-sided Feynman diagrams (DSFDs). In this paper, we restrict the discussion to a two-level system, but the extensions to multiple level systems and systems coupled to other degrees of freedom can be made. Representative DSFDs of various fifth-order nonlinear optical processes in the pump−probe geometry for a two-level system are depicted in Figure 1b using the notation by Hamm.[15] (For each of the processes $R^{(5)}$ that is portrayed in Figure 1b, there are additional DSFDs which are in the excited state population during the waiting time periods. These DSFDs are not depicted here.) We restrict ourselves to diagrams in the observed $\mathbf{k}_{signal} = \mathbf{k}_{probe}$ direction, as well as DSFDs that exhibit only populations during the last waiting times. When using a phase-locked pump pulse train, as delivered by pulse shapers, the emitted signal acquires a phase signature $\phi_{signal} = \alpha\phi_1 + \beta\phi_2 + \gamma\phi_3 + \delta\phi_4$, where α is the number of first pump pulse arrows pointing to the right minus first pump pulse arrows pointing to the left of the DSFDs. Arrows pointing toward the DSFDs represent absorption, while arrows pointing away represent emission. β, γ, and δ can be calculated accordingly for the second, third, and fourth pulse interaction. Practically, we denote the phase signatures in terms of relative phases $\phi_{14} = \phi_1 - \phi_4$, $\phi_{24} = \phi_2 - \phi_4$, and $\phi_{34} = \phi_3 - \phi_4$, since only the interpulse phase relationships matter. In this notation, the overall acquired phase signature of the signal is $\phi_{signal} = \alpha\phi_{14} + \beta\phi_{24} + \gamma\phi_{34}$. As can be seen, δ is in fact not necessary to denote a particular coherence transfer pathway. This stems from the fact that in a pump−probe geometry the system necessarily needs to end in a population state for the second waiting time t_4, which constraints the values of α, β, γ, and δ to be

$$\alpha + \beta + \gamma + \delta = 0 \quad (3)$$

If we furthermore restrict the problem to fifth- and lower-order processes while ignoring higher-order terms, only up to four interactions from the four pump pulses need to be considered. This results in a second condition:

$$|\alpha| + |\beta| + |\gamma| + |\delta| \leq 4 \quad (4)$$

The signals from the four diagrams in Figure 1b in the semi-impulsive limit from eq 2 give

$$\begin{aligned} R_1^{(5)}(t_1, t_2, t_3, t_4, t_5) & \propto \Theta(t_1)\Theta(t_3)\Theta(t_5)\exp(-i\Delta\omega_{10} t_1)\exp(-i\Delta\omega_{10} t_3)\exp(-i\omega_{10} t_5) F_1(t_1, t_2, t_3, t_4, t_5) \\ R_2^{(5)}(t_1, t_2, t_3, t_4, t_5) & \propto \Theta(t_1)\Theta(t_3)\Theta(t_5)\exp(+i\Delta\omega_{10} t_1)\exp(-i\Delta\omega_{10} t_3)\exp(-i\omega_{10} t_5) F_2(t_1, t_2, t_3, t_4, t_5) \\ R_3^{(5)}(t_1, t_2, t_3, t_4, t_5) & \propto \Theta(t_1)\Theta(t_3)\Theta(t_5)\exp(-i\Delta\omega_{10} t_1)\exp(+i\Delta\omega_{10} t_3)\exp(-i\omega_{10} t_5) F_3(t_1, t_2, t_3, t_4, t_5) \\ R_4^{(5)}(t_1, t_2, t_3, t_4, t_5) & \propto \Theta(t_1)\Theta(t_3)\Theta(t_5)\exp(+i\Delta\omega_{10} t_1)\exp(+i\Delta\omega_{10} t_3)\exp(-i\omega_{10} t_5) F_4(t_1, t_2, t_3, t_4, t_5) \end{aligned} \quad (5)$$

dx.doi.org/10.1021/jp4046403 | J. Phys. Chem. B 2013, 117, 15369−15385

where ω_{10} is the resonance frequency of the two-level system and $\Delta\omega_{10} = \omega_{10} - \omega_{ref}$ is the resonance frequency detuned from the reference frequency ω_{ref}. Over t_1 and t_3, the data is collected over a rotating frame at ω_{ref} frequency.[22,23] $\Theta(t)$ is a Heaviside step function. F_1–F_4 are functions that account for dephasing and population relaxation dynamics,[34] and therefore determine the peak shapes. Each coherence transfer pathway contains valuable information, but for purely absorptive spectra which exhibit the highest possible frequency resolution, the overall response function needs to have contributions from all individual response functions $R_1^{(5)}$–$R_4^{(5)}$.[15] A characteristic of using a pump–probe geometry is that all coherence transfer pathways $R_1^{(5)}$–$R_4^{(5)}$ will automatically emit in the same direction $\mathbf{k}_{signal} = \mathbf{k}_{probe}$, which is beneficial for the collection of purely absorptive spectra. However, there is also a multitude of other processes emitted in the $\mathbf{k}_{signal} = \mathbf{k}_{probe}$ direction, of which a few examples are depicted in Figure 1c. They consist of coherence transfer pathways of fifth-order processes, where certain light fields interact more than once with the system, as well as other lower-order processes ($|\alpha| + |\beta| + |\gamma| + |\delta| \leq 2$). Although such processes will not be discriminated by the phase matching condition, they are distinguishable from the desired coherence transfer pathways by their phase signature. The sum of the multitude of undesired processes is denoted with P. One purpose of phase cycling is to get rid of such unwanted signal contributions. In summary, for fixed waiting times t_2 and t_4, the following expression results for the overall phase dependent signal:

$$\begin{aligned} S(t_1, t_3, t_5) \propto\ & R_1^{(5)}(t_1, t_3, t_5) \exp(+i\phi_{14} - i\phi_{24} + i\phi_{34}) \\ & + R_2^{(5)}(t_1, t_3, t_5) \exp(-i\phi_{14} + i\phi_{24} + i\phi_{34}) \\ & + R_3^{(5)}(t_1, t_3, t_5) \exp(+i\phi_{14} - i\phi_{24} - i\phi_{34}) \\ & + R_4^{(5)}(t_1, t_3, t_5) \exp(-i\phi_{14} + i\phi_{24} - i\phi_{34}) + P + \ldots \end{aligned} \tag{6}$$

Experimentally, the first two coherence times t_1 and t_3 are typically collected in the time domain, while the third coherence time t_5 is acquired in the frequency domain by spectrally resolving the signal in a spectrometer, which mathematically is a Fourier transform about the t_5 axis (FT_5). For brevity, we will henceforth drop the waiting time variables t_2 and t_4 in our equations. Subsequent self-heterodyned detection of the signal field with a square-law detector is mathematically equivalent to selecting the real part of the product of the signal field and the intrinsic local oscillator field. In the semi-impulsive limit, the detected frequency resolved signal $\tilde{S}$ can be expressed, using $S(t_1, t_3, t_5)$ of eq 6, as

$$\begin{aligned} & \tilde{S}(\phi_{14}, \phi_{24}, \phi_{34}; t_1, t_3, \omega_5) \\ & \propto \mathrm{Re}[\mathrm{FT}_5\{S(t_1, t_3, t_5)\}] \\ & \equiv \sum_{\alpha,\beta,\gamma} \tilde{s}(\alpha, \beta, \gamma; t_1, t_3, \omega_5) \exp(+i\alpha\phi_{14} + i\beta\phi_{24} + i\gamma\phi_{34}) \end{aligned} \tag{7}$$

The summation in the last line of eq 7 groups all terms according to their phase signature α, β, and γ. Among all possible terms, those of interest are

$$\begin{aligned} & \tilde{s}_{1+4^*}(\alpha = 1, \beta = -1, \gamma = 1; t_1, t_3, \omega_5) \\ & \propto \Theta(t_1)\Theta(t_3) \exp(-i\Delta\omega_{10}t_1) \exp(-i\Delta\omega_{10}t_3) \\ & \quad \times [\tilde{F}_1(t_1, t_3, \omega_5 - \omega_{10}) + \tilde{F}_4^*(t_1, t_3, \omega_5 - \omega_{10})] \end{aligned} \tag{8}$$

$$\begin{aligned} & \tilde{s}_{2+3^*}(\alpha = -1, \beta = 1, \gamma = 1; t_1, t_3, \omega_5) \\ & \propto \Theta(t_1)\Theta(t_3) \exp(+i\Delta\omega_{10}t_1) \exp(-i\Delta\omega_{10}t_3) \\ & \quad \times [\tilde{F}_2(t_1, t_3, \omega_5 - \omega_{10}) + \tilde{F}_3^*(t_1, t_3, \omega_5 - \omega_{10})] \end{aligned} \tag{9}$$

$$\begin{aligned} & \tilde{s}_{3+2^*}(\alpha = 1, \beta = -1, \gamma = -1; t_1, t_3, \omega_5) \\ & \propto \Theta(t_1)\Theta(t_3) \exp(-i\Delta\omega_{10}t_1) \exp(+i\Delta\omega_{10}t_3) \\ & \quad \times [\tilde{F}_3(t_1, t_3, \omega_5 - \omega_{10}) + \tilde{F}_2^*(t_1, t_3, \omega_5 - \omega_{10})] \end{aligned} \tag{10}$$

$$\begin{aligned} & \tilde{s}_{4+1^*}(\alpha = -1, \beta = 1, \gamma = -1; t_1, t_3, \omega_5) \\ & \propto \Theta(t_1)\Theta(t_3) \exp(+i\Delta\omega_{10}t_1) \exp(+i\Delta\omega_{10}t_3) \\ & \quad \times [\tilde{F}_4(t_1, t_3, \omega_5 - \omega_{10}) + \tilde{F}_1^*(t_1, t_3, \omega_5 - \omega_{10})] \end{aligned} \tag{11}$$

where $\tilde{F}_i(t_1, t_3, \omega_5 - \omega_{10}) = \mathrm{FT}_5\{F_i(t_1, t_3, t_5) \exp(-i\omega_{10}t_5)\}$. The asterisk denotes the complex conjugate. Either one of the pair of eqs 8 and 9 or eqs 10 and 11 contains all the relevant terms shown in eq 5 to obtain the pure absorptive peaks in a 3D spectrum. We shall discuss here the choice of an appropriate phase cycling scheme to measure selectively eqs 8 and 9 from the summation series of eq 7.

Mathematically, to extract a specific signal $\tilde{s}(\alpha, \beta, \gamma; t_1, t_3, \omega_5)$ with phase signature $\exp(+i\alpha\phi_{14} + i\beta\phi_{24} + i\gamma\phi_{34})$, a three-dimensional Fourier transform of $\tilde{S}(\alpha, \beta, \gamma; t_1, t_3, \omega_5)$ over the interpulse phase space needs to be performed:

$$\begin{aligned} & \tilde{s}(\alpha, \beta, \gamma; t_1, t_3, \omega_5) \\ & = \int_0^{2\pi}\int_0^{2\pi}\int_0^{2\pi} \mathrm{d}\phi_{14}\, \mathrm{d}\phi_{24}\, \mathrm{d}\phi_{34}\, \tilde{S}(\alpha, \beta, \gamma; t_1, t_3, \omega_5) \\ & \quad \times \exp(-i\alpha\phi_{14}) \exp(-i\beta\phi_{24}) \exp(-i\gamma\phi_{34}) \end{aligned} \tag{12}$$

In our approach, we experimentally sample the phase spaces in discrete steps and eq 12 can be written as a discrete Fourier transform:

$$\begin{aligned} \tilde{s}^{L\times M\times N\times 1}(\alpha, \beta, \gamma; t_1, t_3, \omega_5) &= \frac{1}{LMN} \sum_{l=0}^{L-1}\sum_{m=0}^{M-1}\sum_{n=0}^{N-1} \tilde{S}(l\Delta\phi_{14}, m\Delta\phi_{24}, n\Delta\phi_{34}; t_1, t_3, \omega_5) \exp(-il\alpha\Delta\phi_{14}) \times \exp(-im\beta\Delta\phi_{24}) \\ & \quad \times \exp(-in\gamma\Delta\phi_{34}) \\ &\equiv \frac{1}{LMN} \sum_{l=0}^{L-1}\sum_{m=0}^{M-1}\sum_{n=0}^{N-1} \tilde{S}(l\Delta\phi_{14}, m\Delta\phi_{24}, n\Delta\phi_{34}; t_1, t_3, \omega_5) W_L^{l\alpha} W_M^{m\beta} W_N^{n\gamma} \end{aligned} \tag{13}$$

dx.doi.org/10.1021/jp4046403 | J. Phys. Chem. B 2013, 117, 15369–15385

where $\phi_{14} = l\Delta\phi_{14}$, $\phi_{24} = m\Delta\phi_{24}$, and $\phi_{34} = n\Delta\phi_{34}$, L is the number of sample points in the ϕ_{14}-phase space, M is the number of sample points in the ϕ_{24}-phase space, and N is the number of sample points in the ϕ_{34}-phase space. $W_L^{l\alpha}$, $W_M^{m\beta}$, and $W_N^{n\gamma}$ are the respective summation weights. Experimentally, this means a series of experiments need to be conducted with different interpulse phases ϕ_{14}, ϕ_{24}, and ϕ_{34}, and the resultant series of phase dependent signals added according to the weights $W_L^{l\alpha}$, $W_M^{m\beta}$, and $W_N^{n\gamma}$. For a $L \times M \times N \times 1$ phase cycling scheme, it is desirable to keep L, M, and N minimal, as this determines the total number of measurements that need to be performed. In principle, it does not matter which one of the four pulses we should reference the pulse phases to. Therefore, the resultant signals from a $L \times M \times N \times 1$ phase cycling experiment and a $1 \times L \times M \times N$ experiment are the same, the latter being if we reference the interpulse phases to the first pulse. In this article, we have referenced it to the last pulse as it is simpler to set up experimentally.

Phase cycling is a technique that is analogous to theoretical methods developed by research groups to extract relevant terms from a nonperturbative calculation of nonlinear optical signals.[35−37]

A related technique to phase cycling can be found in phase modulated 2D fluorescence spectroscopy and related experiments.[38−40] In this technique, instead of phase cycling through the laser pulses with discrete phase steps, phases are introduced in a continuously fashion and the desired signal with its corresponding phase modulation signature can be obtained using a lock-in detector.

The general conditions of eqs 3 and 4 allow 55 coherence transfer pathways (see the Supporting Information) to evolve without phase cycling. The phase cycling scheme discussed in this article is similar in nature to the phase cycling schemes of 2D collinear optical spectroscopy discussed in an earlier article.[29] In the 2D collinear optical spectroscopy discussed in ref 29, four interactions with the four collinear pulses lead to a population state which is then detected. After the consideration of aliasing, both rephasing and non-rephasing spectra can be obtained using a $1 \times 3 \times 3 \times 3$ phase cycling scheme. In this present article, the first four interactions with the four pump pulses lead to a population which is then probed by the fifth interaction. The conditions denoted in eqs 3 and 4 are therefore the same as that presented in ref 29 with a four-pulse train. Likewise, a full 27 steps $1 \times 3 \times 3 \times 3$ (or a $3 \times 3 \times 3 \times 1$) phase cycling scheme can be performed and the appropriate linear combination of the signals provided by eq 13 can then be applied to extract the signals $\tilde{s}_{1+4*}(\alpha = -1, \beta = 1, \gamma = 1; t_1, t_3, \omega_5)$ and $\tilde{s}_{2+3*}(\alpha = -1, \beta = 1, \gamma = 1; t_1, t_3, \omega_5)$ (eqs 8 and 9, respectively) (the $3 \times 3 \times 3 \times 1$ phase cycling scheme to select $\tilde{s}(\alpha, \beta, \gamma; t_1, t_3, \omega_5)$ is listed in full detail in the Supporting Information).

Upon obtaining the signal of eqs 8 and 9 using the $3 \times 3 \times 3 \times 1$ phase cycling scheme where the first three pulses are each cycled over phases ϕ_{14}, ϕ_{24}, and $\phi_{34} = 0$, $2\pi/3$, and $4\pi/3$, we explain here how the data can then be processed to obtain pure absorptive peaks. We make the following simplification that $F_1(t_1, t_3, t_5) = F_2(t_1, t_3, t_5) = F_3(t_1, t_3, t_5) = F_4(t_1, t_3, t_5) = F(t_1, t_3, t_5)$ are real functions and $F(t_1, t_3, t_5) = F(t_1, t_3)F(t_5) = F(t_1)F(t_3)F(t_5)$. These assumptions are only made for brevity to illustrate in a clearer fashion how pure absorptive peak shapes are obtained. More general expressions may be written if required. We can express the Fourier transform of $F(t_j)$ about any coherence time axis t_j, where $j = 1$, 3, or 5, as $\mathrm{FT}_j\{\Theta(t_j)\ \exp(-i\omega_{10}t_j)\} = A(\omega_j - \omega_{10}) + iD(\omega_j - \omega_{10})$, where $A(\omega_j - \omega_{10})$ and $D(\omega_j - \omega_{10})$ are the absorptive and dispersive terms, respectively. Fourier transformations of eq 8 about t_1 and t_3 and taking the real part of the signal only then results in a 3D spectrum:

$$\begin{aligned}
\tilde{s}_{1+4*}^{3\times3\times3\times1}(\alpha = 1, \beta = -1, \gamma = 1; \omega_1, \omega_3, \omega_5) &= \mathrm{Re}\{\mathrm{FT}_{1,3}\{\tilde{s}_{1+4*}(\alpha = 1, \beta = -1, \gamma = 1; t_1, t_3, \omega_5)\}\} \\
&= \mathrm{Re}\{\mathrm{FT}_{1,3}\{F(t_1)F(t_3)\ \exp(-i\Delta\omega_{01}t_1 - i\Delta\omega_{01}t_3)A(\omega_5 - \omega_{10})\}\} \\
&= \mathrm{Re}\left\{\begin{matrix}[A(\omega_1 - \Delta\omega_{10}) + iD(\omega_1 - \Delta\omega_{10})] \times \\ [A(\omega_3 - \Delta\omega_{10}) + iD(\omega_3 - \Delta\omega_{10})]A(\omega_5 - \omega_{10})\end{matrix}\right\} \\
&= A(\omega_1 - \Delta\omega_{10})A(\omega_3 - \Delta\omega_{10})A(\omega_5 - \omega_{10}) \\
&\quad - D(\omega_1 - \Delta\omega_{10})D(\omega_3 - \Delta\omega_{10})A(\omega_5 - \omega_{10})
\end{aligned} \tag{14}$$

From this expression, we can see that the spectrum will be centered at $(\omega_1, \omega_3, \omega_5) = (\Delta\omega_{10}, \Delta\omega_{10}, \omega_{10})$. Also, it is apparent that the spectrum still contains dispersive contributions along ω_1 and ω_3. Similarly, the 3D spectrum resulting from $\tilde{s}_{2+3*}(\alpha = -1, \beta = 1, \gamma = 1; t_1, t_3, \omega_5)$ of eq 9 becomes

$$\begin{aligned}
\tilde{s}_{2+3^*}^{3\times3\times3\times1}(\alpha = -1, \beta = 1, \gamma = 1; \omega_1, \omega_3, \omega_5) &= \mathrm{Re}\{\mathrm{FT}_{1,3}\{\tilde{s}_{2+3*}(\alpha = -1, \beta = 1, \gamma = 1; t_1, t_3, \omega_5)\}\} \\
&= \mathrm{Re}\{\mathrm{FT}_{1,3}\{F(t_1)F(t_3)\exp(i\Delta\omega_{01}t_1 - i\Delta\omega_{01}t_3)A_5(\omega_5 - \omega_{10})\}\} \\
&= \mathrm{Re}\left\{\begin{matrix}[A(\omega_1 + \Delta\omega_{10}) + iD(\omega_1 + \Delta\omega_{10})] \times \\ [A(\omega_3 - \Delta\omega_{10}) + iD(\omega_3 - \Delta\omega_{10})]A(\omega_5 - \omega_{10})\end{matrix}\right\} \\
&= A(\omega_1 + \Delta\omega_{10})A(\omega_3 - \Delta\omega_{10})A(\omega_5 - \omega_{10}) \\
&\quad - D(\omega_1 + \Delta\omega_{10})D(\omega_3 - \Delta\omega_{10})A(\omega_5 - \omega_{10})
\end{aligned} \tag{15}$$

dx.doi.org/10.1021/jp4046403 | J. Phys. Chem. B 2013, 117, 15369−15385

We note that the signal now is centered at $(\omega_1, \omega_3, \omega_5) = (-\Delta\omega_{10}, \Delta\omega_{10}, \omega_{10})$. The peaks arising from eqs 14 and 15 lie in different quadrants of the $\omega_5 = \omega_{10}$ plane in a 3D Cartesian coordinate system. Upon reflecting eq 15 about the $\omega_1 = 0$ plane, we obtain the mirrored spectrum:

$$\begin{aligned}&\tilde{s}_{2+3^*}^{3\times3\times3\times1,M(\omega_1)}(\alpha=-1,\beta=1,\gamma=1;\omega_1,\omega_3,\omega_5)\\&\quad=A(\omega_1-\Delta\omega_{10})A(\omega_3-\Delta\omega_{10})A(\omega_5-\omega_{10})\\&\qquad+D(\omega_1-\Delta\omega_{10})D(\omega_3-\Delta\omega_{10})A(\omega_5-\omega_{10})\end{aligned}\tag{16}$$

Equations 14 and 16 can then be summed up to cancel out the remaining dispersive features by obeying the assumption made earlier, leading to only the purely absorptive spectrum:

$$\begin{aligned}&\tilde{s}_{1+2+3+4}^{3\times3\times3\times1}(\omega_1,\omega_3,\omega_5)\\&\quad=\tilde{s}_{1+4^*}(\alpha=1,\beta=-1,\gamma=1;\omega_1,\omega_3,\omega_5)\\&\qquad+\tilde{s}_{2+3^*}^{M(\omega_1)}(\alpha=-1,\beta=1,\gamma=1;\omega_1,\omega_3,\omega_5)\\&\quad=A(\omega_1-\Delta\omega_{10})A(\omega_3-\Delta\omega_{10})A(\omega_5-\omega_{10})\end{aligned}\tag{17}$$

We will now discuss the application of a $2 \times 2 \times 2 \times 1$ phase cycling scheme. In a $2 \times 2 \times 2 \times 1$ phase cycling scheme, the first three pulses are each cycled over phases ϕ_{14}, ϕ_{24}, and $\phi_{34} = 0$ and π. A two-step phase cycle cannot discriminate between summation weightings $\exp(i\phi)$ and $\exp(-i\phi)$ due to aliasing.[29] Therefore, by applying a $2 \times 2 \times 2 \times 1$ phase cycling scheme and using eq 7 to select the signal $\tilde{s}_{1+4^*}(\alpha = 1, \beta = -1, \gamma = 1; t_1, t_3, \omega_5)$ of eq 8 with phase signature $\exp(+i\phi_{14} - i\phi_{24} + i\phi_{34})$, we will not be able to exclude signals from signals $\tilde{s}_{2+3^*}(\alpha = -1, \beta = 1, \gamma = 1; t_1, t_3, \omega_5)$, $\tilde{s}_{3+2^*}(\alpha = 1, \beta = -1, \gamma = -1; t_1, t_3, \omega_5)$, and $\tilde{s}_{4+1^*}(\alpha = -1, \beta = 1, \gamma = -1; t_1, t_3, \omega_5)$ of eqs 9, 10, and 11, with phase signatures $\exp(-i\phi_{14} + i\phi_{24} + i\phi_{34})$, $\exp(+i\phi_{14} - i\phi_{24} - i\phi_{34})$, and $\exp(-i\phi_{14} + i\phi_{24} - i\phi_{34})$, respectively. Fourier transformations about t_1 and t_3 of this $2 \times 2 \times 2 \times 1$ phase cycled signal that consist of the sum of eqs 8−11 followed by taking the real part will give

$$\begin{aligned}\tilde{s}^{2\times2\times2\times1}(\omega_1,\omega_3,\omega_5)&=\mathrm{Re}\left\{\mathrm{FT}_{1,3}\begin{Bmatrix}\tilde{s}_{1+4^*}(\alpha=1,\beta=-1,\gamma=1;t_1,t_3,\omega_5)\\+\tilde{s}_{2+3^*}(\alpha=-1,\beta=1,\gamma=1;t_1,t_3,\omega_5)\\+\tilde{s}_{3+2^*}(\alpha=1,\beta=-1,\gamma=-1;t_1,t_3,\omega_5)\\+\tilde{s}_{4+1^*}(\alpha=-1,\beta=1,\gamma=-1;t_1,t_3,\omega_5)\end{Bmatrix}\right\}\\&=\mathrm{Re}\left\{\mathrm{FT}_{1,3}\begin{Bmatrix}F(t_1)F(t_3)\exp(-i\Delta\omega_{01}t_1-i\Delta\omega_{01}t_3)A(\omega_5-\omega_{10})\\+F(t_1)F(t_3)\exp(+i\Delta\omega_{01}t_1-i\Delta\omega_{01}t_3)A(\omega_5-\omega_{10})\\+F(t_1)F(t_3)\exp(-i\Delta\omega_{01}t_1+i\Delta\omega_{01}t_3)A(\omega_5-\omega_{10})\\+F(t_1)F(t_3)\exp(+i\Delta\omega_{01}t_1+i\Delta\omega_{01}t_3)A(\omega_5-\omega_{10})\end{Bmatrix}\right\}\\&=\mathrm{Re}\left\{\begin{Bmatrix}[A(\omega_1-\Delta\omega_{10})+iD(\omega_1-\Delta\omega_{10})][A(\omega_3-\Delta\omega_{10})+iD(\omega_3-\Delta\omega_{10})]A(\omega_5-\omega_{10})\\+[A(\omega_1+\Delta\omega_{10})+iD(\omega_1+\Delta\omega_{10})][A(\omega_3-\Delta\omega_{10})+iD(\omega_3-\Delta\omega_{10})]A(\omega_5-\omega_{10})\\+[A(\omega_1-\Delta\omega_{10})+iD(\omega_1-\Delta\omega_{10})][A(\omega_3+\Delta\omega_{10})+iD(\omega_3+\Delta\omega_{10})]A(\omega_5-\omega_{10})\\+[A(\omega_1+\Delta\omega_{10})+iD(\omega_1+\Delta\omega_{10})][A(\omega_3+\Delta\omega_{10})+iD(\omega_3+\Delta\omega_{10})]A(\omega_5-\omega_{10})\end{Bmatrix}\right\}\\&=A(\omega_1-\Delta\omega_{10})A(\omega_3-\Delta\omega_{10})A(\omega_5-\omega_{10})-D(\omega_1-\Delta\omega_{10})D(\omega_3-\Delta\omega_{10})A(\omega_5-\omega_{10})\\&\quad+A(\omega_1+\Delta\omega_{10})A(\omega_3-\Delta\omega_{10})A(\omega_5-\omega_{10})-D(\omega_1+\Delta\omega_{10})D(\omega_3-\Delta\omega_{10})A(\omega_5-\omega_{10})\\&\quad+A(\omega_1-\Delta\omega_{10})A(\omega_3+\Delta\omega_{10})A(\omega_5-\omega_{10})-D(\omega_1-\Delta\omega_{10})D(\omega_3+\Delta\omega_{10})A(\omega_5-\omega_{10})\\&\quad+A(\omega_1+\Delta\omega_{10})A(\omega_3+\Delta\omega_{10})A(\omega_5-\omega_{10})-D(\omega_1+\Delta\omega_{10})D(\omega_3+\Delta\omega_{10})A(\omega_5-\omega_{10})\end{aligned}\tag{18}$$

This resultant 3D spectrum will have four peaks, each at the four different quadrants of the $\omega_5 = \omega_{10}$ plane, $(\omega_1, \omega_3, \omega_5) = (\Delta\omega_{10}, \Delta\omega_{10}, \omega_{10})$, $(\omega_1, \omega_3, \omega_5) = (-\Delta\omega_{10}, \Delta\omega_{10}, \omega_{10})$, $(\omega_1, \omega_3, \omega_5) = (\Delta\omega_{10}, -\Delta\omega_{10}, \omega_{10})$, and $(\omega_1, \omega_3, \omega_5) = (-\Delta\omega_{10}, -\Delta\omega_{10}, \omega_{10})$, respectively. Upon reflecting eq 18 about the $\omega_1 = 0$ plane, we have

$$\begin{aligned}&\tilde{s}^{2\times2\times2\times1,M(\omega_1)}(\omega_1,\omega_3,\omega_5)\\&\quad=A(\omega_1+\Delta\omega_{10})A(\omega_3-\Delta\omega_{10})A(\omega_5-\omega_{10})\\&\qquad+D(\omega_1+\Delta\omega_{10})D(\omega_3-\Delta\omega_{10})A(\omega_5-\omega_{10})\\&\qquad+A(\omega_1-\Delta\omega_{10})A(\omega_3-\Delta\omega_{10})A(\omega_5-\omega_{10})\\&\qquad+D(\omega_1-\Delta\omega_{10})D(\omega_3-\Delta\omega_{10})A(\omega_5-\omega_{10})\\&\qquad+A(\omega_1+\Delta\omega_{10})A(\omega_3+\Delta\omega_{10})A(\omega_5-\omega_{10})\\&\qquad+D(\omega_1+\Delta\omega_{10})D(\omega_3+\Delta\omega_{10})A(\omega_5-\omega_{10})\\&\qquad+A(\omega_1-\Delta\omega_{10})A(\omega_3+\Delta\omega_{10})A(\omega_5-\omega_{10})\\&\qquad+D(\omega_1-\Delta\omega_{10})D(\omega_3+\Delta\omega_{10})A(\omega_5-\omega_{10})\end{aligned}\tag{19}$$

And adding the spectrum (eq 18) to its mirror image (eq 19) yields a 3D spectrum that contains peaks that are purely absorptive:

$$\begin{aligned}&\tilde{s}_{1+2+3+4}^{2\times2\times2\times1}(\omega_1,\omega_3,\omega_5)\\&\quad=A(\omega_1-\Delta\omega_{10})A(\omega_3-\Delta\omega_{10})A(\omega_5-\omega_{10})\\&\qquad+A(\omega_1+\Delta\omega_{10})A(\omega_3-\Delta\omega_{10})A(\omega_5-\omega_{10})\\&\qquad+A(\omega_1-\Delta\omega_{10})A(\omega_3+\Delta\omega_{10})A(\omega_5-\omega_{10})\\&\qquad+A(\omega_1+\Delta\omega_{10})A(\omega_3+\Delta\omega_{10})A(\omega_5-\omega_{10})\end{aligned}\tag{20}$$

The four purely absorptive peaks of the 3D spectrum are identical and separated by $2\Delta\omega_{10}$. In practice, $\Delta\omega_{10}$ can be experimentally manipulated with the pulse shaper so that the four identical peaks are well separated. It is therefore sufficient to show only one quadrant of the 3D spectrum. We should note here that reflecting eq 18 about the $\omega_3 = 0$ plane and the subsequent adding of the spectra will give the same outcome.

dx.doi.org/10.1021/jp4046403 | J. Phys. Chem. B 2013, 117, 15369−15385

We have recently demonstrated the measurement of this purely absorptive 3D spectrum.[25] For samples with a congested or broad spectrum with a bandwidth on the order of $2\Delta\omega_{10}$, the aliased signals will overlap in a 2 × 2 × 2 × 1 phase cycling scheme. To overcome this problem of aliasing, we have to either increase $\Delta\omega_{10}$ by changing ω_{ref} to a further displaced frequency, or we can choose a 3 × 3 × 3 × 1 phase cycling scheme. In a multileveled or coupled system, a 2 × 2 × 2 × 1 phase cycling scheme is insufficient to remove undesired signals such as two-quantum absorption signals from $\tilde{s}_{2Q1}(\alpha = 1, \beta = 1, \gamma = -1; \omega_1, \omega_3, \omega_5)$ and $\tilde{s}_{2Q2}(\alpha = -1, \beta = -1, \gamma = 1; \omega_1, \omega_3, \omega_5)$, which will appear at $(\omega_1, \omega_3, \omega_5) = (-2\Delta\omega_{10}, \Delta\omega_{10}, \omega_{10})$ and $(\omega_1, \omega_3, \omega_5) = (2\Delta\omega_{10}, -\Delta\omega_{10}, \omega_{10})$, respectively. This necessitates a 3 × 3 × 3 × 1 phase cycling scheme to select the desired signal. However, if there are no peaks appearing in a 3 × 3 × 3 × 1 phase cycling scheme when choosing $\tilde{s}(\alpha = 1, \beta = 1, \gamma = -1)$ and $\tilde{s}(\alpha = -1, \beta = -1, \gamma = 1)$, we can assume that both of the undesired pathways do not contribute significantly to the overall signal, and a 2 × 2 × 2 × 1 phase cycling scheme can be used.

B. Separating Signals R_1, R_2, R_3, and R_4 in Phase Cycled 3D Spectra. The signals $\tilde{s}_{1+4*}(\alpha = 1, \beta = -1, \gamma = 1; t_1, t_3, \omega_5)$, $\tilde{s}_{2+3*}(\alpha = -1, \beta = 1, \gamma = 1; t_1, t_3, \omega_5)$, $\tilde{s}_{3+2*}(\alpha = 1, \beta = -1, \gamma = -1; t_1, t_3, \omega_5)$, and $\tilde{s}_{4+1*}(\alpha = -1, \beta = 1, \gamma = -1; t_1, t_3, \omega_5)$ of eqs 8−11 each contain two terms from eq 5. In order to selectively measure only one single term R_1, R_2, R_3, or R_4 from eq 5, the collected signals of eq 7 need to be mathematically treated before phase cycling schemes are applied. This procedure is similar to what is done to separate the rephasing and non-rephasing signal from a purely absorptive 2D spectrum by subjecting the data to the causality condition.[21,23] The signal $\tilde{s}_{1+4*}(\alpha = 1, \beta = -1, \gamma = 1; t_1, t_3, \omega_5)$ shown in eq 8 is part of the total signal of eq 7 and contains R_1 and R_4 components. Using $\tilde{s}_{1+4*}$ as an example, the procedures to impose causality to achieve the resultant signal will be demonstrated. The first step is to inverse Fourier transform about ω_5, and eq 8 will become:

$$\begin{aligned}\tilde{s}^{C}_{1+4*}(\alpha = 1, \beta = -1, \gamma = 1; t_1, t_3, t_5) &= \Theta(t_1)\Theta(t_3)\Theta(t_5)F_1(t_1, t_3, t_5)\exp(-i\Delta\omega_{10}t_1) \\ &\times \exp(-i\Delta\omega_{10}t_3) + \Theta(t_1)\Theta(t_3)\Theta(-t_5)F_4^{*}(t_1, t_3, -t_5) \\ &\times \exp(-i\Delta\omega_{10}t_1)\exp(-i\Delta\omega_{10}t_3) \end{aligned} \quad (21)$$

By imposing causality, any signal that arrives before $t = 0$ fs is discarded and hence terms containing $\Theta(-t)$ are removed from eq 21. We note that the R_4 term will be removed from eq 21. The remaining signal is back Fourier transformed with respect to t_5 to give

$$\begin{aligned}\tilde{s}^{C}_{1}(\alpha = 1, \beta = -1, \gamma = 1; t_1, t_3, \omega_5) &\propto \Theta(t_1)\Theta(t_3)\exp(-i\Delta\omega_{10}t_1)\exp(-i\Delta\omega_{10}t_3) \\ &\times \tilde{F}_1(t_1, t_3, \omega_5 - \omega_{10}) \end{aligned} \quad (22)$$

This process of imposing causality is applied on the experimentally collected signal of eq 7, and the resultant processed signal will be denoted as $\tilde{S}^{C}(\phi_{14} + \phi_{24} + \phi_{34}; t_1, t_3, \omega_5)$. Analogous to eq 22, the terms in eqs 9−11 that are also present in eq 7 upon imposing causality will become, respectively,

$$\begin{aligned}\tilde{s}^{C}_{2}(\alpha = -1, \beta = 1, \gamma = 1; t_1, t_3, \omega_5) &\propto \Theta(t_1)\Theta(t_3)\exp(+i\Delta\omega_{10}t_1)\exp(-i\Delta\omega_{10}t_3) \\ &\times \tilde{F}_2(t_1, t_3, \omega_5 - \omega_{10}) \end{aligned} \quad (23)$$

$$\begin{aligned}\tilde{s}^{C}_{3}(\alpha = 1, \beta = -1, \gamma = -1; t_1, t_3, \omega_5) &\propto \Theta(t_1)\Theta(t_3)\exp(-i\Delta\omega_{10}t_1)\exp(+i\Delta\omega_{10}t_3) \\ &\times \tilde{F}_3(t_1, t_3, \omega_5 - \omega_{10}) \end{aligned} \quad (24)$$

$$\begin{aligned}\tilde{s}^{C}_{4}(\alpha = -1, \beta = 1, \gamma = -1; t_1, t_3, \omega_5) &\propto \Theta(t_1)\Theta(t_3)\exp(+i\Delta\omega_{10}t_1)\exp(+i\Delta\omega_{10}t_3) \\ &\times \tilde{F}_4(t_1, t_3, \omega_5 - \omega_{10}) \end{aligned} \quad (25)$$

Now, using the 3 × 3 × 3 × 1 phase cycling scheme to extract $\tilde{s}^{C}_{1}(\alpha = 1, \beta = -1, \gamma = 1; t_1, t_3, \omega_5)$ of eq 22 from the causality imposed signal $\tilde{S}^{C}(\phi_{14} + \phi_{24} + \phi_{34}; t_1, t_3, \omega_5)$ followed by Fourier transformation about t_1 and t_3 will give $\tilde{F}_1(\omega_1 - \Delta\omega_{10}, \omega_3 - \Delta\omega_{10}, \omega_5 - \omega_{10}; t_2, t_4)$ which is the 3D Fourier transform of the $R_1^{(5)}$ process as described in eq 5. Similarly, the 3 × 3 × 3 × 1 phase cycling scheme can extract the $\tilde{s}^{C}_{2}(\alpha = -1, \beta = 1, \gamma = 1; \omega_1, \omega_3, \omega_5)$, $\tilde{s}^{C}_{3}(\alpha = 1, \beta = -1, \gamma = -1; t_1, t_3, \omega_5)$, and $\tilde{s}^{C}_{4}(\alpha = -1, \beta = 1, \gamma = -1; \omega_1, \omega_3, \omega_5)$ terms of eqs 23, 24, and 25, respectively, from $\tilde{S}^{C}(\phi_{14} + \phi_{24} + \phi_{34}; t_1, t_3, \omega_5)$ to give $\tilde{F}_2(\omega_1 + \Delta\omega_{10}, \omega_3 - \Delta\omega_{10}, \omega_5 - \omega_{10}; t_2, t_4)$, $\tilde{F}_3(\omega_1 - \Delta\omega_{10}, \omega_3 + \Delta\omega_{10}, \omega_5 - \omega_{10}; t_2, t_4)$, and $\tilde{F}_4(\omega_1 + \Delta\omega_{10}, \omega_3 + \Delta\omega_{10}, \omega_5 - \omega_{10}; t_2, t_4)$.

When one uses the 2 × 2 × 2 × 1 phase cycling scheme to attempt to recover $\tilde{s}^{C}_{1}(\alpha = 1, \beta = -1, \gamma = 1; t_1, t_3, \omega_5)$, as explained in the previous section, one cannot distinguish between signals with phase terms with phase signatures $\exp(+i\phi_{14} - i\phi_{24} + i\phi_{34})$, $\exp(-i\phi_{14} + i\phi_{24} + i\phi_{34})$, $\exp(+i\phi_{14} - i\phi_{24} - i\phi_{34})$, and $\exp(-i\phi_{14} + i\phi_{24} - i\phi_{34})$. The resultant signal when similarly Fourier transformed about t_1 and t_3 gives

$$\begin{aligned}\tilde{s}^{C,2\times2\times2\times1}(\omega_1, \omega_3, \omega_5) &= \tilde{F}_1(\omega_1 - \Delta\omega_{10}, \omega_3 - \Delta\omega_{10}, \omega_5 - \omega_{10}; t_2, t_4) \\ &+ \tilde{F}_2(\omega_1 + \Delta\omega_{10}, \omega_3 - \Delta\omega_{10}, \omega_5 - \omega_{10}; t_2, t_4) \\ &+ \tilde{F}_3(\omega_1 - \Delta\omega_{10}, \omega_3 + \Delta\omega_{10}, \omega_5 - \omega_{10}; t_2, t_4) \\ &+ \tilde{F}_4(\omega_1 + \Delta\omega_{10}, \omega_3 + \Delta\omega_{10}, \omega_5 - \omega_{10}; t_2, t_4) \end{aligned} \quad (26)$$

where the signals for $\tilde{s}^{C,2\times2\times2\times1}_{1}(\alpha = 1, \beta = -1, \gamma = 1; \omega_1, \omega_3, \omega_5)$, $\tilde{s}^{C,2\times2\times2\times1}_{2}(\alpha = -1, \beta = 1, \gamma = 1; \omega_1, \omega_3, \omega_5)$, $\tilde{s}^{C,2\times2\times2\times1}_{3}(\alpha = 1, \beta = -1, \gamma = -1; \omega_1, \omega_3, \omega_5)$, and $\tilde{s}^{C,2\times2\times2\times1}_{4}(\alpha = -1, \beta = 1, \gamma = -1; \omega_1, \omega_3, \omega_5)$ are all retrieved in a single 3D spectrum. Each of the four processes will be in a different quadrant on the $\omega_5 = \omega_{10}$ plane. The real part of the summation of the four causality imposed signals upon proper mirror imaging will yield a purely absorptive signal.

III. EXPERIMENT

The experimental setup has been described in detail elsewhere.[23,25] Briefly, a 1 kHz titanium sapphire regenerative amplifier pumps a home-built optical parametric amplifier (OPA) to generate pulses centered at 665 nm, with a bandwidth of 16 nm, as shown in Figure 2.

The pulses were compressed by an acousto-optic programmable dispersive filter (AOPDF) (Dazzler) to a duration of 50 fs.

dx.doi.org/10.1021/jp4046403 | J. Phys. Chem. B 2013, 117, 15369−15385

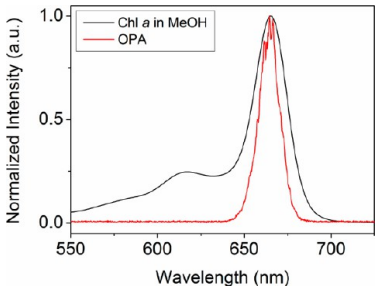

Figure 2. A linear absorption spectrum of chlorophyll *a* in methanol (black) with the excitation pulse spectrum of the OPA (red) coinciding with the Q_y transition.

The 3D experimental setup was based on a pump−probe beam geometry, where the first four pump pulses interacted collinearly, while the last interaction from the probe pulse interacted at a small crossing angle. In the experiment, a four-pulse train (12 nJ per pulse) was created by the AOPDF with variable delays t_1, t_2, and t_3 between pulses 1 and 2, pulses 2 and 3, and pulses 3 and 4, respectively. A whitelight continuum was created from a sapphire window to form pulse 5. The waiting time t_4 was the delay between pulses 4 and 5, and was set by a mechanical translation stage. We note that, as the whitelight continuum probe is chirped, a different frequency in the whitelight continuum will have a different delay t_4, which may lead to distortion in the spectra.[41] This problem can be overcome with post-data chirp-correction by characterization of the chirp and adjusting the delay of the corresponding wavelength accordingly.[42] Delays t_1 and t_3 were coherence times, while t_2 and t_4 were population times. The fifth-order signal is emitted in the same direction as pulse 5, and was heterodyne-detected by pulse 5 and frequency-resolved by a spectrometer (PIXIS 100B) to form the emission axis ω_5. Chlorophyll *a* (Chl *a*) was dissolved in methanol and placed in a 1 mm sapphire cell, and the linear absorption spectrum is shown in Figure 2. An optical density of 0.2 is measured for the sample at 665 nm. It is known that distortions in multidimensional spectrum features can be due to sample thickness and the non-collinear phase matching beam geometry used in most multidimensional spectroscopic setups.[43−45] We believe that a pump probe configuration such as ours where four out of five interacting pulses are interacting collinearly will have less spectral distortions compared to a fully non-collinear phase matching beam geometry. In our 3D spectrum, the distortion due to sample thickness is expected to be present and can be reduced by reducing the sample thickness.

To obtain a 3D spectrum, both coherence times t_1 and t_3 were scanned from 0 to 140 fs in 10 fs time steps. The population times t_2 and t_4 were kept fixed. The reference wavelength of the pulse shaper was set to 715 nm, such that the Nyquist limit was 15 fs for both the t_1 and t_3 axes, and the difference between the peak absorption of the sample and the reference wavelength was $\Delta\omega_{10}$ = 31 THz. To perform phase cycling, for every step taken for the coherence time, the relative phases of the first three pulses, ϕ_1, ϕ_2, and ϕ_3, were varied with respect to ϕ_4. For the 2 × 2 × 2 × 1 phase cycling scheme, the phases were cycled between $\phi_j = 0$ and π, while, for the 3 × 3 × 3 × 1 phase cycling scheme, the phases were cycled with $\phi_j = 0$, $2\pi/3$, and $4\pi/3$, where j = 1, 2, and 3 for both schemes. Scattered light from the pump beam is removed by subtracting the signal with and without the probe beam using a 500 Hz chopper. To ensure that the pulse train was created accurately, power measurements were made to ensure comparability when phases of the pulses were cycled. A 2 × 2 × 2 × 1 or 3 × 3 × 3 × 1 phase cycling scheme is performed on the emitted fifth-order signal by systematic weighted summation as described in eq 13. The phase cycled data was then zero-padded up to 85 data points and Fourier transformed with respect to t_1 and t_3 to give a 3D spectrum with signals $\tilde{s}_{1+4^*}(\alpha = 1, \beta = -1, \gamma = 1)$ and $\tilde{s}_{3+2^*}(\alpha = 1, \beta = -1, \gamma = -1)$ without any undesired peaks, as shown in eqs 14 and 15. The addition of the mirror image of the spectrum to itself yielded the purely absorptive 3D spectrum. To retrieve signals $\tilde{s}_1(\alpha = 1, \beta = -1, \gamma = 1)$, $\tilde{s}_2(\alpha = -1, \beta = 1, \gamma = 1)$, $\tilde{s}_3(\alpha = 1, \beta = -1, \gamma = -1)$, and $\tilde{s}_4(\alpha = -1, \beta = 1, \gamma = -1)$, we modified the phase cycling data treatment by imposing causality to the collected data as described in eqs 21 and 22.[21,23]

IV. RESULTS

Without phase cycling, or with insufficient phase cycling, the detected spectrum would be contaminated with spurious peaks due to undesired processes (lower-order signals, pump−probe signals, etc.) as denoted by P in eq 6 and due to aliasing caused by undersampling of the discrete Fourier transform denoted in eq 13. In the following, we will discuss the 3D spectra that are obtained when we apply a different phase cycling scheme to choose the term $\tilde{s}(\alpha = 1, \beta = -1, \gamma = 1; t_1, t_3, \omega_5)$ from the signal of eq 7. In Figure 3, we present various phase cycling schemes that are insufficient to select the desired signal.

In Figure 3a, the spectrum depicted is measured without any phase cycling, or in the language of phase cycling, a 1 × 1 × 1 × 1 phase cycling scheme. The isosurfaces in Figure 3a are drawn at an intensity ∼2500 times that of the desired fifth-order signals (signals presented in Figure 4 onward). It is dominated by a peak from a first-order linear signal of negative amplitude at position $(\omega_1, \omega_3, \omega_5) = (0, 0, \omega_{10})$. This signal arises from zero interactions with the first four pulses and one interaction from the fifth "probe" pulse. Third-order and fifth-order signals are also present but are less intense than the first-order signal, and hence, they do not show up in the spectrum. The desired fifth-order signals at $(\omega_1, \omega_3, \omega_5) = (\Delta\omega_{10}, \Delta\omega_{10}, \omega_{10})$ remain unobserved under these intense first-order contributions. In Figure 3b, the 2 × 2 × 1 × 1 phase cycling scheme removes the first-order signal but is unable to remove the third-order signals at $(\omega_1, \omega_3, \omega_5) = (\pm\Delta\omega_{10}, 0, \omega_{10})$. This arises from the insufficient phase cycling of the third pulse. The signals that have no interaction with the third and fourth pulses are not eliminated. The third-order signals observed at $(\omega_1, \omega_3, \omega_5) = (\pm\Delta\omega_{10}, 0, \omega_{10})$ arise after an interaction each with the first and second pulse followed by an interaction with the fifth "probe" pulse. The isosurfaces in Figure 3b are drawn at an intensity ∼10 times that of the isosurfaces in Figure 4a. Figure 4 depicts the isosurfaces of the 3D spectrum obtained from a 2 × 2 × 2 × 1 phase cycling scheme, shown in eq 18, at (t_2, t_4) = (400 fs, 300 fs). Using this phase cycling scheme, all the first- and third-order signals are eliminated, and only fifth-order signals remain. In Figure 4a, the 3D spectrum has four peaks labeled as I, II, III, and IV and they are located in the separate quadrants on the plane of $\omega_5 = \omega_{10}$ = 451 THz at $(\omega_1, \omega_3, \omega_5) = (\Delta\omega_{10}, \Delta\omega_{10}, \omega_{10})$, $(\omega_1, \omega_3, \omega_5) = (-\Delta\omega_{10}, \Delta\omega_{10}, \omega_{10})$, $(\omega_1, \omega_3, \omega_5) = (\Delta\omega_{10}, -\Delta\omega_{10}, \omega_{10})$, and $(\omega_1, \omega_3, \omega_5) = (-\Delta\omega_{10}, -\Delta\omega_{10}, \omega_{10})$, respectively.

As mentioned in the earlier section II.A with eq 18, the peaks II, III, and IV arise from aliasing. One major concern of

dx.doi.org/10.1021/jp4046403 | J. Phys. Chem. B 2013, 117, 15369−15385

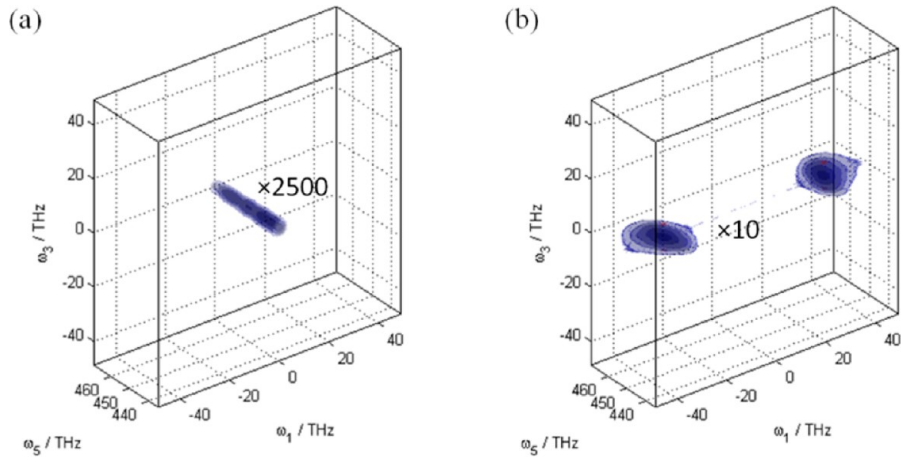

Figure 3. Isosurfaces of 3D spectra from insufficient phase cycling steps that results in unwanted signals. (a) Signals from a 1 × 1 × 1 × 1 phase cycling scheme. The first-order signal at $(\omega_1, \omega_3, \omega_5) = (0, 0, \omega_{10})$ dominates the spectrum and is ∼2500 times more intense than the fifth-order signal (Figure 4). (b) A 2 × 2 × 1 × 1 phase cycling scheme results in the unwanted third-order signals at $(\omega_1, \omega_3, \omega_5) = (\pm\Delta\omega_{10}, 0, \omega_{10})$, which is ∼10 times more intense than the fifth-order signal (Figure 4).

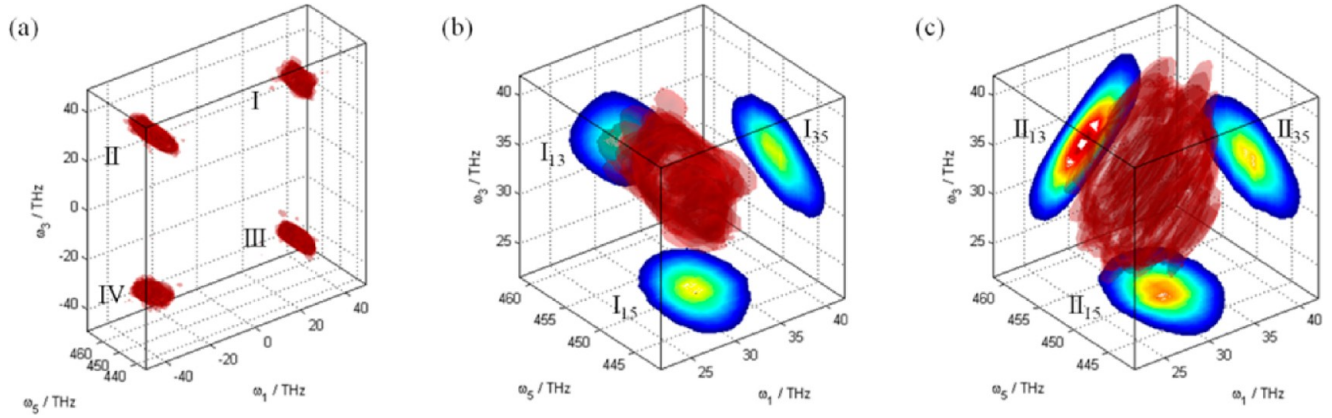

Figure 4. Isosurfaces of 3D spectra from a 2 × 2 × 2 × 1 phase cycling scheme with t_2 = 400 fs and t_4 = 300 fs. Only the peaks from fifth-order processes remain. (a) Peaks I, II, III, and IV represent signals $\tilde{s}_{1+4^*}$, $\tilde{s}_{2+3^*}$, $\tilde{s}_{3+2^*}$, and $\tilde{s}_{4+1^*}$, respectively. (b) A magnified view of peak I with 2D projections depicted on the grid plane. The 2D projection, I_{13}, is "phase-twisted", while I_{35} and I_{15} have purely absorptive peak shapes. (c) A magnified view of peak II, with the mirror image taken across $\omega_1 = 0$ to display the signal in a quadrant with an all-positive frequency axis. The 2D projection II_{13} is phase-twisted, while II_{35} and II_{15} have purely absorptive peak shapes.

aliasing is the possibility of overlapped aliased signals. Here, the reference signal was chosen to ensure that the peaks I, II, III, and IV are well separated in the 3D spectrum by $2\Delta\omega_{10}$ = 62 THz so that there are no ambiguities in peak assignment. An enlarged 3D spectrum of peak I from Figure 4a is depicted in Figure 4b. Figure 4c depicts an enlarged 3D spectrum of peak II after a mirror image of it is taken about the $\omega_1 = 0$ axis. We will explain in a later section why the mirror image is obtained. The 2D projections of these peaks are also presented on the walls of the grid and labeled. To show that the peaks in the 3D spectrum are indeed the fifth-order signals as expected, we provide here the analysis to the positions and features of the observed 3D peaks. Since 3D peaks are difficult to visualize on a piece of paper, we use 2D projections of the 3D peaks for analysis.

Peak I (Figure 4a) and the mirror imaged peak II (Figure 4b) can be described in terms of the absorptive and dispersive components extracted from the first term of eq 18 and the second term of eq 19, respectively, and they are expressed as

$$\tilde{s}_{\mathrm{I}}^{2\times2\times2\times1}(\omega_1, \omega_3, \omega_5) \propto A(\omega_1 - \Delta\omega_{10})A(\omega_3 - \Delta\omega_{10})A(\omega_5 - \omega_{10}) - D(\omega_1 - \Delta\omega_{10})D(\omega_3 - \Delta\omega_{10})A(\omega_5 - \omega_{10}) \quad (27)$$

$$\tilde{s}_{\mathrm{II}}^{2\times2\times2\times1,M(\omega_1)}(\omega_1, \omega_3, \omega_5) \propto A(\omega_1 - \Delta\omega_{10})A(\omega_3 - \Delta\omega_{10})A(\omega_5 - \omega_{10}) + D(\omega_1 - \Delta\omega_{10})D(\omega_3 - \Delta\omega_{10})A(\omega_5 - \omega_{10}) \quad (28)$$

The features of the projections can be simulated by integrating the above functions over the appropriate axis. The 2D projection onto the (ω_1, ω_3) axis that corresponds to the 2D projections I_{13} and II_{13} from Figure 4b and c, respectively, is achieved by integrating eqs 27 and 28, respectively, over ω_5. Since the absorptive and dispersion components are symmetric and antisymmetric, respectively, the results are

dx.doi.org/10.1021/jp4046403 | J. Phys. Chem. B 2013, 117, 15369−15385

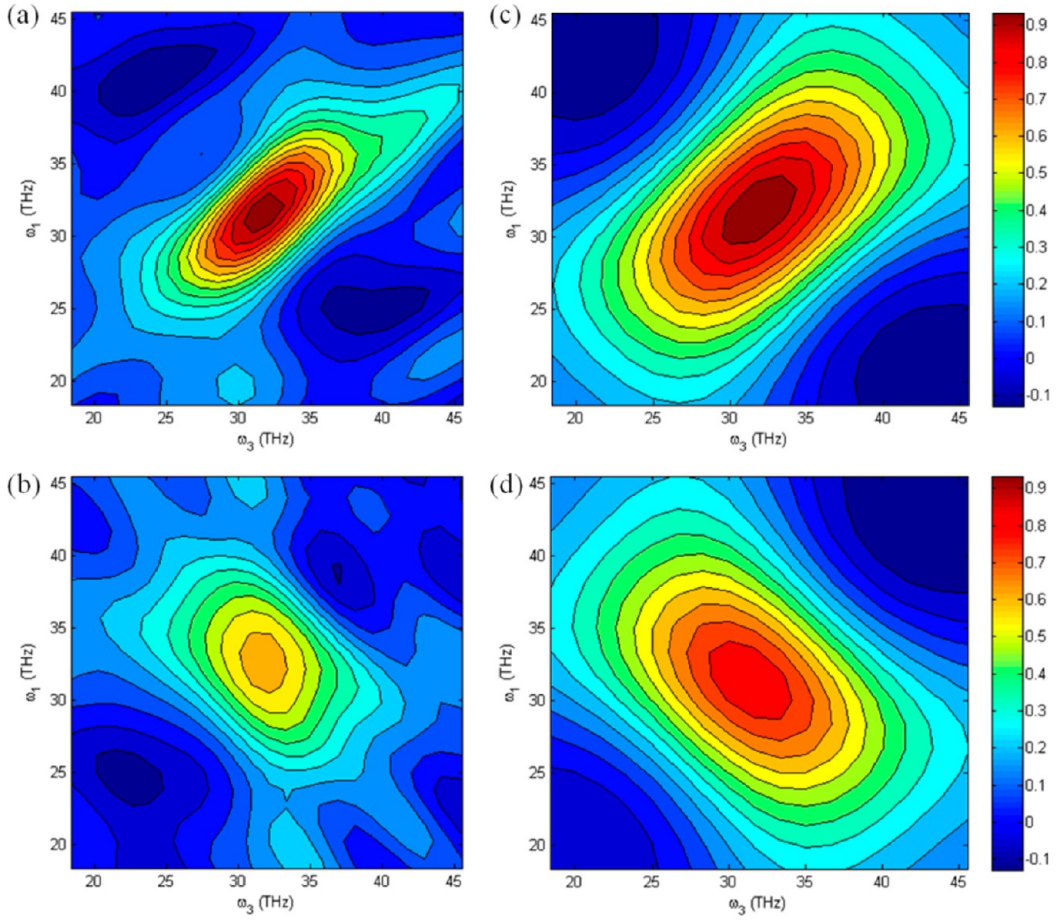

Figure 5. Comparison of the 2D projections I_{13} and II_{13} from Figure 4 with simulated 2D projections. The phase-twisted feature is evident in both experimental and simulated results. As the simulation did not consider finite bandwidth of the interacting pulses, the resultant line widths in the experimental projections are smaller as compared to the simulated spectra. (a) 2D projection I_{13}. (b) 2D projection II_{13}. (c) Simulated 2D projection I_{13}. (d) Simulated 2D projection II_{13}.

$$\tilde{s}_{I_{13}}^{2\times2\times2\times1}(\omega_1, \omega_3) \propto A(\omega_1 - \Delta\omega_{10})A(\omega_3 - \Delta\omega_{10}) - D(\omega_1 - \Delta\omega_{10}) \times D(\omega_3 - \Delta\omega_{10}) \quad (29)$$

$$\tilde{s}_{II_{13}}^{2\times2\times2\times1,M(\omega_1)}(\omega_1, \omega_3) \propto A(\omega_1 - \Delta\omega_{10})A(\omega_3 - \Delta\omega_{10}) + D(\omega_1 - \Delta\omega_{10}) \times D(\omega_3 - \Delta\omega_{10}) \quad (30)$$

These peaks on the 2D projection will appear with distinctive "phase-twisted" shapes, where the peak broadens outward along the diagonal (or antidiagonal) axis and hence appears twisted.[6,46] These "phase-twisted" shapes are due to dispersive contributions $D(\omega_1 - \Delta\omega_{10})D(\omega_3 - \Delta\omega_{10})$ in eqs 29 and 30 and have a bigger footprint on spectra compared to purely absorptive peaks (described by, for example, eqs 31−34). The peaks corresponding to eqs 29 and 30 correspond to the rephasing and non-rephasing peaks, respectively, from 2D spectroscopy.[2,6,46] In Figure 5a and b, the 2D projections I_{13} and II_{13} from Figure 4b and c are depicted, respectively. The phase-twisted feature can be seen in the peaks. In the previous section, it is theoretically shown that peak I contains a signal from the R_1 and R_4 processes (eq 8), while peak II contains signals from the R_2 and R_3 processes (eq 9).

To show that the experimental 3D spectra is consistent with the derivations, the response functions R_1, R_2, R_3, and R_4[15] were calculated and the corresponding 3D spectra and 2D projections were generated. The two-point frequency fluctuation correlation function of Chl *a* in methanol was obtained from experiment.[47] These simulated 2D projections are presented in Figure 5c and d. The simulation did not take into consideration the finite temporal pulse width of the interacting pulses, and hence, the simulated 2D projections are broader than the experimental 2D projections which were obtained using a pulse width of ∼60 fs. However, phase-twisted features from both simulation and experiment are clearly consistent.

We now discuss the other 2D projections I_{15}, I_{35}, II_{15}, and II_{35}. Integrating over ω_3 for eqs 27 and 28, the resultant signals are

$$\tilde{s}_{I_{15}}^{2\times2\times2\times1}(\omega_1, \omega_5) \propto A(\omega_1 - \Delta\omega_{10})A(\omega_5 - \Delta\omega_{10}) \quad (31)$$

$$\tilde{s}_{II_{15}}^{2\times2\times2\times1,M(\omega_1)}(\omega_1, \omega_5) \propto A(\omega_1 - \Delta\omega_{10})A(\omega_5 - \Delta\omega_{10}) \quad (32)$$

By integrating over ω_1 for eqs 27 and 28, we have

$$\tilde{s}_{I_{35}}^{2\times2\times2\times1}(\omega_3, \omega_5) \propto A(\omega_3 - \Delta\omega_{10})A(\omega_5 - \Delta\omega_{10}) \quad (33)$$

$$\tilde{s}_{II_{35}}^{2\times2\times2\times1,M(\omega_1)}(\omega_3, \omega_5) \propto A(\omega_3 - \Delta\omega_{10})A(\omega_5 - \Delta\omega_{10}) \quad (34)$$

dx.doi.org/10.1021/jp4046403 | J. Phys. Chem. B 2013, 117, 15369−15385

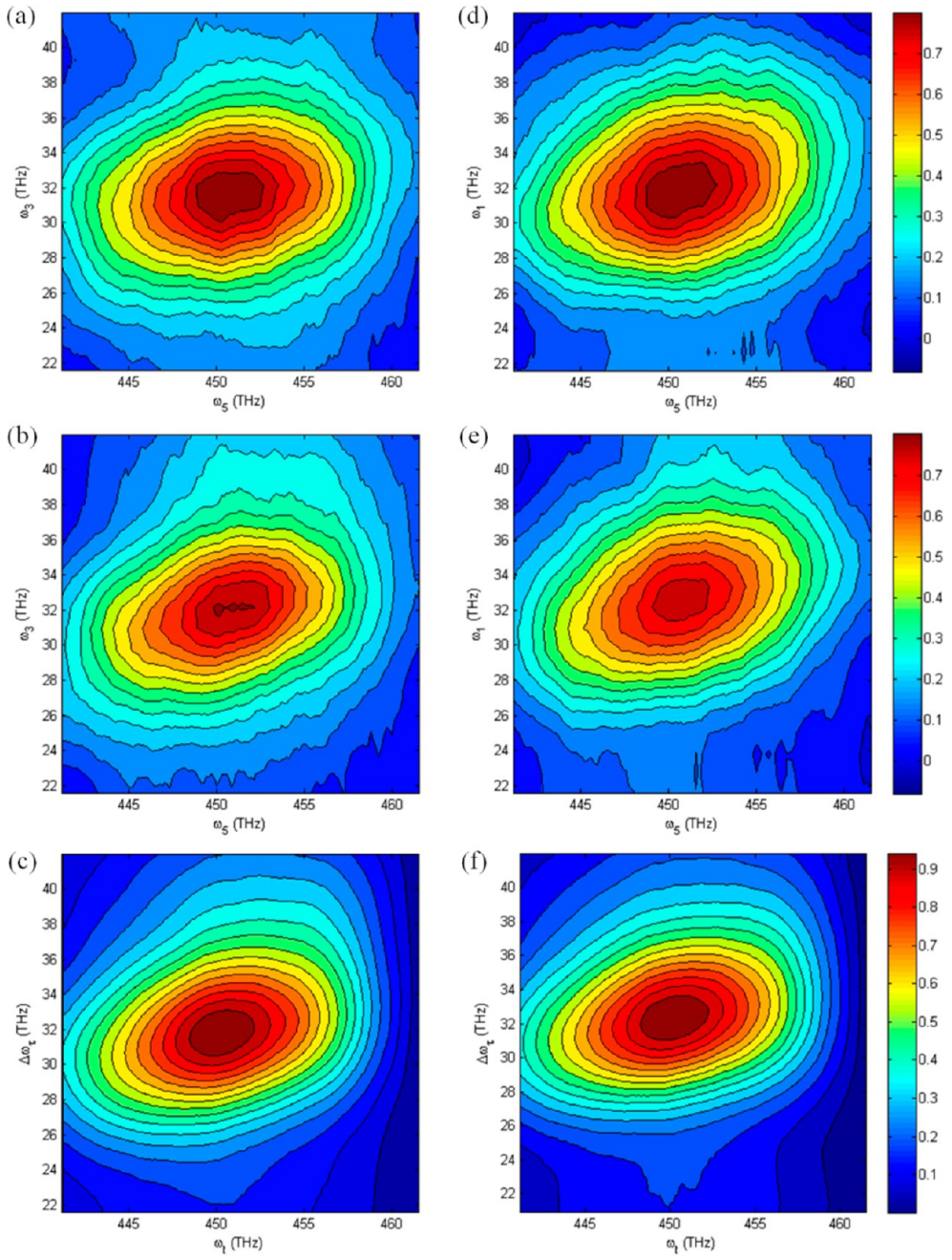

Figure 6. Comparison of the 2D projections from Figure 4 with experimental 2D spectra. All the 2D projections show similar purely absorptive peak shapes as those obtained in 2D spectra. (a) 2D projection, I_{35}. (b) 2D projection, II_{35}. (c) 2D spectrum at T_w = 300 fs. (d) 2D projection of I_{15}. (e) 2D projection of II_{15}. (f) 2D spectrum at T_w = 700 fs.

All these 2D projections have purely absorptive peak shapes and should look similar. In Figure 6, the 2D projections I_{15}, I_{35}, II_{15}, and II_{35} from Figure 4a and b are presented.

As can be seen, the shapes are absorptive and similar, in contrast to the peak shapes in Figure 5a and b. In Figure 6c and f, the experimental purely absorptive 2D spectra of chlorophyll *a* at T_w = 400 fs and T_w = 700 fs are depicted as an example to show that the I_{15}, I_{35}, II_{15}, and II_{35} are indeed purely absorptive line shapes, in contrast to the phase-twisted features of I_{13} and II_{13} of Figure 5c and d.

As mentioned in section II.A, the 3D spectrum from a 2 × 2 × 2 × 1 phase cycling scheme can be manipulated to produce a purely absorptive 3D spectrum. This has been demonstrated in our earlier paper.[25] In Figure 7a, the purely absorptive 3D spectrum is obtained by the summation of Figure 4a and its mirror image about $\omega_3 = 0$.

This summed 3D spectrum contains four purely absorptive peaks described in eq 20 that are mirror imaged replicas of each other. In Figure 7b, we present the peak from the $(+\omega_1, +\omega_3, +\omega_5)$-octant, together with the 2D projections on the grid wall that show purely absorptive features.

In Figure 8a, the 3D spectra obtained from a 3 × 3 × 3 × 1 phase cycling scheme that chooses the signal $\tilde{s}_{1+4^*}^{3\times3\times3\times1}(\alpha = 1, \beta = -1, \gamma = 1)$ is depicted.

The peak is centered at $(\omega_1, \omega_3, \omega_5) = (+\Delta\omega_{10}, +\Delta\omega_{10}, \omega_{10})$, as predicted in eq 14, and is the same as peak I in Figure 4a. Comparing Figure 8a with Figure 4a, one can also see that the

dx.doi.org/10.1021/jp4046403 | J. Phys. Chem. B 2013, 117, 15369−15385

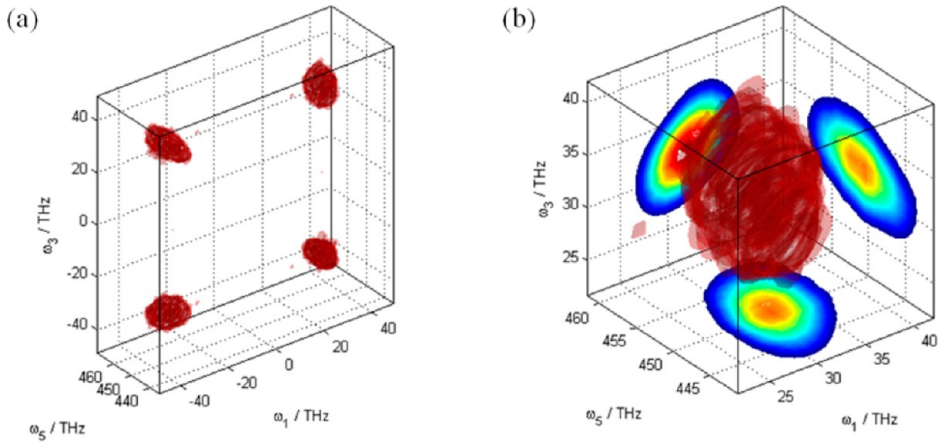

Figure 7. (a) Purely absorptive peaks obtained from a 2 × 2 × 2 × 1 phase cycling scheme by summing up Figure 4a and its mirror image taken across $\omega_1 = 0$. (b) A magnified view of the peak in the $(+\omega_1, +\omega_3, +\omega_5)$-octant, with the respective 2D projections at the grid plane.

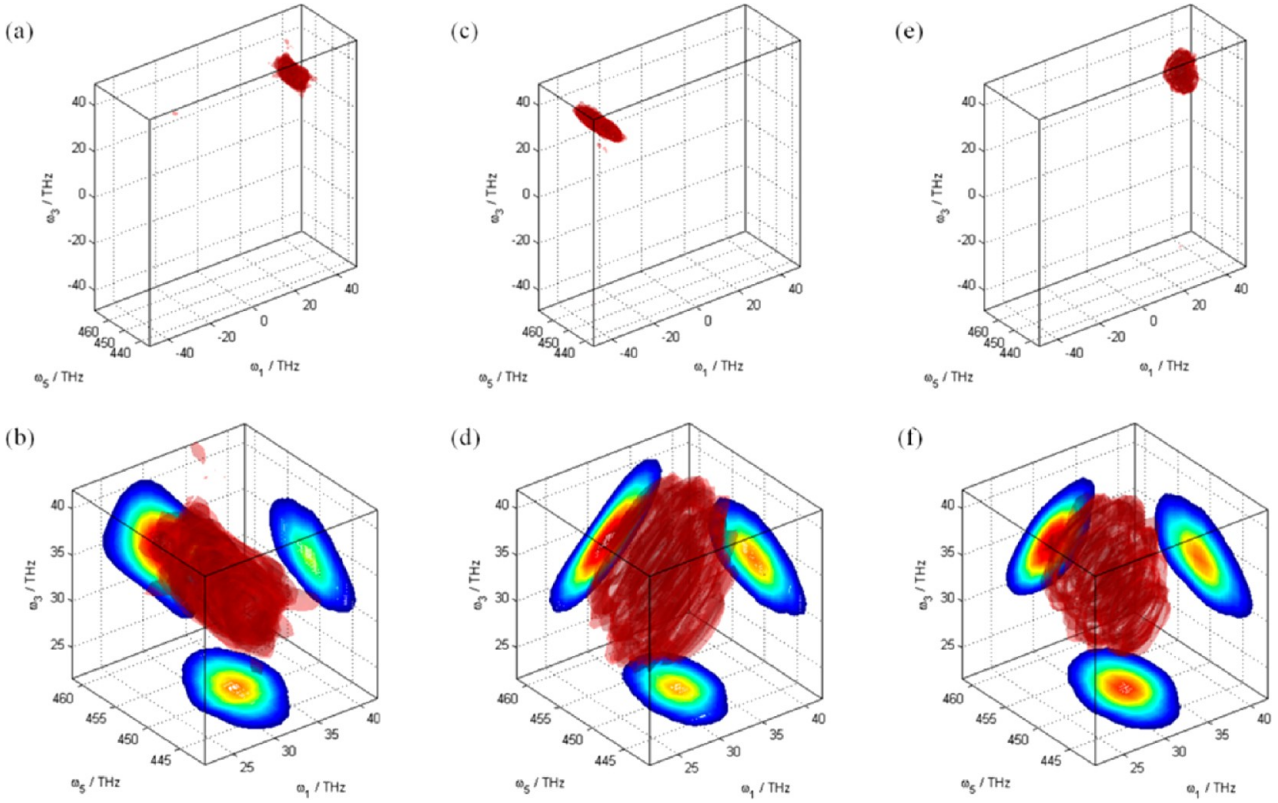

Figure 8. Isosurfaces of 3D spectra from 3 × 3 × 3 × 1 phase cycling schemes. (a) The signal is the same as peak I of Figure 4a and represents $\tilde{s}_{1+4*}$. (b) A close-up view of part a, with the respective 2D projections on the grid plane. (c) The signal is the same as peak II of Figure 4a and represents $\tilde{s}_{2+3*}$. (d) A magnified spectrum of part c mirror imaged across $\omega_1 = 0$ onto the positive axis quadrant, and the corresponding 2D projections. (e) A purely absorptive peak obtained from the summation of part a and the mirror image of part b across $\omega_1 = 0$. (f) A magnified view of part e. The 2D projections show purely absorptive peak shapes on all three grid planes of the cube.

3 × 3 × 3 × 1 phase cycling scheme is able to selectively choose the terms $\tilde{s}_{1+4*}(\alpha = 1, \beta = -1, \gamma = 1)$ without the signals $\tilde{s}_{2+3*}(\alpha = -1, \beta = 1, \gamma = 1)$, $\tilde{s}_{3+2*}(\alpha = 1, \beta = -1, \gamma = -1)$, or $\tilde{s}_{4+1*}(\alpha = -1, \beta = 1, \gamma = -1)$ that arises from aliasing. Figure 8b depicts an enlarged spectrum from Figure 8a, and the 2D projections at the face of the grid cube are comparable to those of Figure 4b. Using the same 3 × 3 × 3 × 1 = 27 data set but in a different linear combination, the signal $\tilde{s}_{2+3*}^{3\times3\times3\times1}(\alpha = -1, \beta = 1, \gamma = 1)$ can then be chosen and the 3D spectrum is depicted in Figure 8c. The peak is located at $(\omega_1, \omega_3, \omega_5) = (-\Delta\omega_{10}, \Delta\omega_{10}, \omega_{10})$, as predicted in eq 15. In Figure 8d, the magnified view of Figure 8c is presented in the positive frequency octant by taking the mirror image about the $\omega_1 = 0$ axis. The 2D projections can be compared to Figure 4c and are shown to be similar. From these examples, the validity of the phase cycling schemes for 3D optical spectroscopy is shown experimentally. Upon summing both signals from Figure 8a and the mirror image of Figure 8c about the $\omega_1 = 0$ plane, as prescribed by eq 17, we obtain, in Figure 8e, a purely absorptive signal that is similar to the peak from the

dx.doi.org/10.1021/jp4046403 | J. Phys. Chem. B 2013, 117, 15369−15385

$(+\omega_1, +\omega_3, +\omega_5)$-octant in Figure 7a. In Figure 8f, the close-up view of Figure 8e and 2D projections are similar to those in Figure 7b.

To retrieve the signals from individual coherence pathways R_1, R_2, R_3, and R_4 in Figure 1, causality is imposed before applying a phase cycling scheme as described in section II.B. Figure 9 depicts the 3D spectrum that is obtained from a causality imposed 2 × 2 × 2 × 1 phase cycling scheme, which is described in eq 26. Figure 9a contains the isosurfaces of four peaks I^c, II^c, III^c, and IV^c which represent the processes R_1, R_2, R_3, and R_4, respectively.

We compare Figure 9a with Figure 4a. In Figure 4a, peaks I and IV are similar, as they contain both processes R_1 and R_4, while peaks II and III are similar, as they contain both processes R_2 and R_3. However, in Figure 9a, the imposing of causalities has separated all the processes and they each occupy a separate quadrant. A close-up view of peaks I^c, II^c, III^c, and IV^c is depicted in Figure 9b−e, respectively, where mirror images of the figures are taken about $\omega_1 = 0$ and/or $\omega_3 = 0$ planes when applicable so that the peaks will appear in the positive frequency octant $(+\omega_1, +\omega_3, +\omega_5)$. For consistency, Figure 9f shows a purely absorptive peak that is obtained by the sum of parts b−e of Figure 9. As expected, it can be seen to be similar to Figures 7b and 8f.

For a causality imposed 3 × 3 × 3 × 1 phase cycling scheme, the signals for $\tilde{s}_1^{C,3\times3\times3\times1}(\alpha = 1, \beta = -1, \gamma = 1)$, $\tilde{s}_2^{C,3\times3\times3\times1}(\alpha = -1, \beta = 1, \gamma = 1)$, $\tilde{s}_3^{C,3\times3\times3\times1}(\alpha = 1, \beta = -1, \gamma = -1)$, and $\tilde{s}_4^{C,3\times3\times3\times1}(\alpha = -1, \beta = 1, \gamma = -1)$ are shown in Figure 10a−d, respectively, and they are located at the same positions as the retrieved signals from a causality imposed 2 × 2 × 2 × 1 phase cycling scheme of Figure 9a.

The enlarged 3D spectra and the 2D projections of the respective signals are shown in Figure 10e−h. It can be observed that the phase-twisted features look comparable to Figure 9b−e, according to eqs 22−25. By summing $\tilde{s}_1^{C,3\times3\times3\times1}(\alpha = 1, \beta = -1, \gamma = 1)$, $\tilde{s}_2^{C,3\times3\times3\times1}(\alpha = -1, \beta = 1, \gamma = 1)$, $\tilde{s}_3^{C,3\times3\times3\times1}(\alpha = 1, \beta = -1, \gamma = -1)$, and $\tilde{s}_4^{C,3\times3\times3\times1}(\alpha = 1, \beta = 1, \gamma = -1)$, as shown in eq 17, we will obtain the purely absorptive peak as shown in Figure 8f.

Figure 11 shows the 2D projections of the 3D spectrum for the R_1 process shown in Figure 10a.

Here, the theoretical derivation for R_1 is presented as an example to predict the peak shape of the signal and compare it with the experimental result. With the simplification that was used in section II.A that $F(t_1, t_3, t_5) = F(t_1, t_3)F(t_5) = F(t_1)F(t_3)F(t_5)$ and that $\mathrm{FT}_j\{\Theta(t_j)F(t_j)\exp(-i\omega_{10}t_j)\} = A(\omega_j - \omega_{10}) + iD(\omega_j - \omega_{10})$, we obtain from eq 22, after Fourier transform, the real part of the 3D spectrum that is due to the R_1 process which can be expressed as

$$\tilde{s}_1^{C,3\times3\times3\times1}(\alpha = 1, \beta = -1, \gamma = 1; \omega_1, \omega_3, \omega_5) \propto \mathrm{Re}\begin{Bmatrix}[A(\omega_1 - \Delta\omega_{10}) + iD(\omega_1 - \Delta\omega_{10})] \\ \times[A(\omega_3 - \Delta\omega_{10}) + iD(\omega_3 - \Delta\omega_{10})] \\ \times[A(\omega_5 - \omega_{10}) + iD(\omega_5 - \omega_{10})]\end{Bmatrix}$$

$$\begin{aligned} &= A(\omega_1 - \Delta\omega_{10})A(\omega_3 - \Delta\omega_{10})A(\omega_5 - \omega_{10}) \\ &\quad - D(\omega_1 - \Delta\omega_{10})D(\omega_3 - \Delta\omega_{10})A(\omega_5 - \omega_{10}) \\ &\quad - D(\omega_1 - \Delta\omega_{10})A(\omega_3 - \Delta\omega_{10})D(\omega_5 - \omega_{10}) \\ &\quad - A(\omega_1 - \Delta\omega_{10})D(\omega_3 - \Delta\omega_{10})D(\omega_5 - \omega_{10}) \end{aligned} \tag{35}$$

In order to obtain the 2D projections onto (ω_1, ω_3), (ω_3, ω_5), and (ω_1, ω_5) planes, eq 35 is integrated over ω_5, ω_1, and ω_3, respectively. The three resultant expressions are

$$\begin{aligned} &\tilde{s}_{I_{13}}^{C,3\times3\times3\times1}(\omega_1, \omega_3) \\ &\quad = A(\omega_1 - \Delta\omega_{10})A(\omega_3 - \Delta\omega_{10}) - D(\omega_1 - \Delta\omega_{10}) \\ &\qquad \times D(\omega_3 - \Delta\omega_{10}) \end{aligned} \tag{36}$$

$$\begin{aligned} &\tilde{s}_{I_{35}}^{C,3\times3\times3\times1}(\omega_3, \omega_5) \\ &\quad = A(\omega_3 - \Delta\omega_{10})A(\omega_5 - \omega_{10}) - D(\omega_3 - \Delta\omega_{10}) \\ &\qquad \times D(\omega_5 - \omega_{10}) \end{aligned} \tag{37}$$

$$\begin{aligned} &\tilde{s}_{I_{15}}^{C,3\times3\times3\times1}(\omega_1, \omega_5) \\ &\quad = A(\omega_1 - \Delta\omega_{10})A(\omega_5 - \omega_{10}) - D(\omega_1 - \Delta\omega_{10}) \\ &\qquad \times D(\omega_5 - \omega_{10}) \end{aligned} \tag{38}$$

All three expressions are similar with phase-twisted features, and it proves that the experimental data obtained for R_1 shown in Figure 10a is consistent with the theoretical derivation. By working out the equations, it can be shown that all 2D projections for $\tilde{s}_{II}^{C,3\times3\times3\times1}$, $\tilde{s}_{III}^{C,3\times3\times3\times1}$, and $\tilde{s}_{IV}^{C,3\times3\times3\times1}$ are phase-twisted as well, which is in good agreement with Figure 10e−h, and the case is also true for the 3D spectrum from a causality implemented 2 × 2 × 2 × 1 phase cycling scheme, as shown in Figure 9b−e.

V. CASCADING THIRD-ORDER CONTRIBUTIONS TO THE FIFTH-ORDER SIGNAL

In higher-order nonlinear spectroscopy, there might be undesired third-order cascades that appear in the same phase-matched direction as the desired fifth-order signal, while having the same intensity dependence. This is evident in fifth-order Raman spectroscopy, where the experiments were contaminated with third-order signals.[48−50] It is therefore important to determine the contributions of third-order cascades to the fifth-order signals. Third-order cascades occur when the third-order polarization response created by three pulse interactions is reabsorbed by the sample to produce a second third-order polarization response after interactions with the remaining two pulses. Sequential and parallel cascades are two types of third-order cascades that can result in an overall fifth-order signal.[7,51] The contribution of the third-order cascades is dependent on the optical density of the sample and phase-matching geometry. A way to verify the contribution of cascaded third-order signals

dx.doi.org/10.1021/jp4046403 | J. Phys. Chem. B 2013, 117, 15369−15385

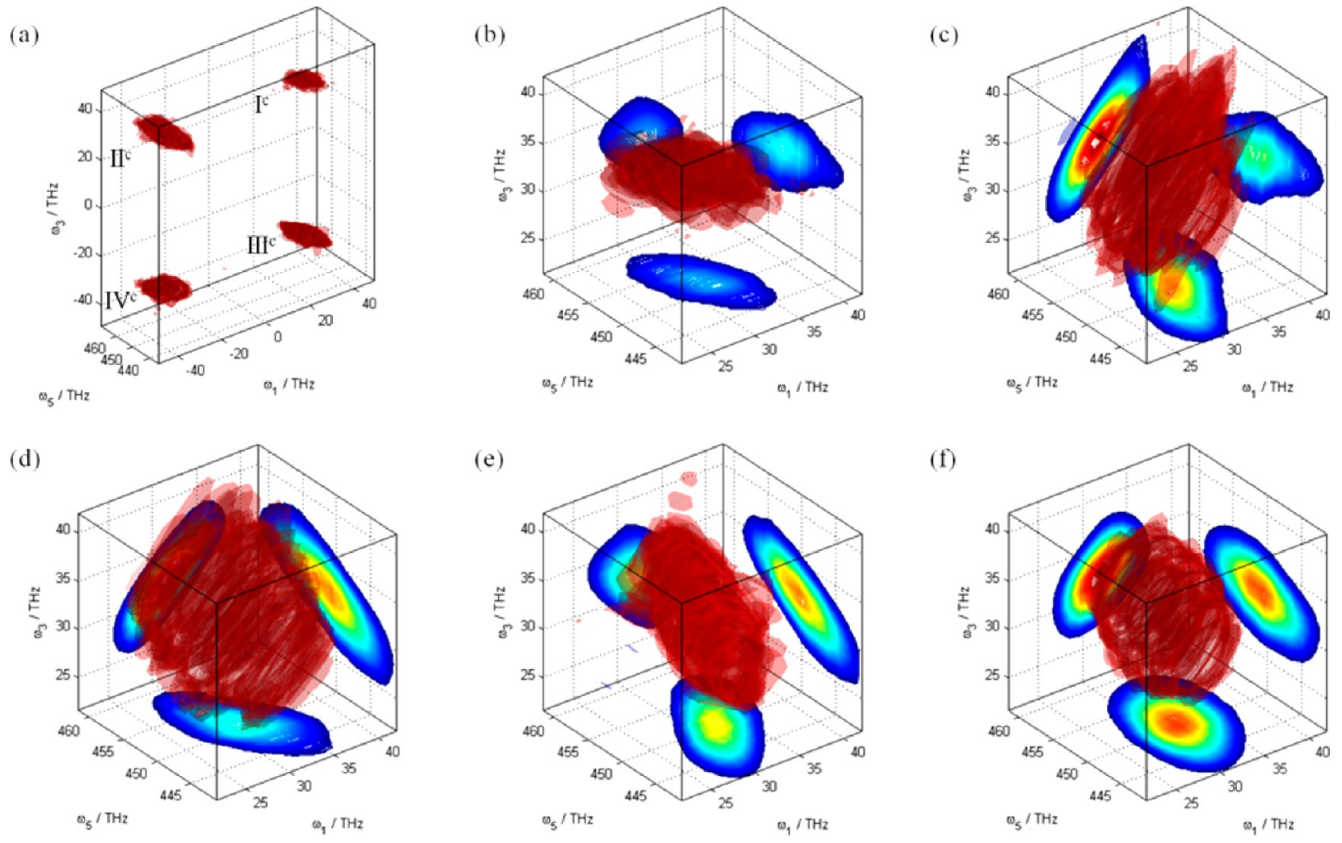

Figure 9. (a) 3D spectra of a causality imposed 2 × 2 × 2 × 1 phase cycling scheme. Magnified views and 2D projections of (b) I^c, (c) II^c, (d) III^c, and (e) IV^c. All magnified spectra of II^c, III^c, and IV^c are mirror imaged onto the positive quadrant. The 2D projections all show phase-twisted features. (f) By summing up parts b−e, a purely absorptive spectrum is obtained.

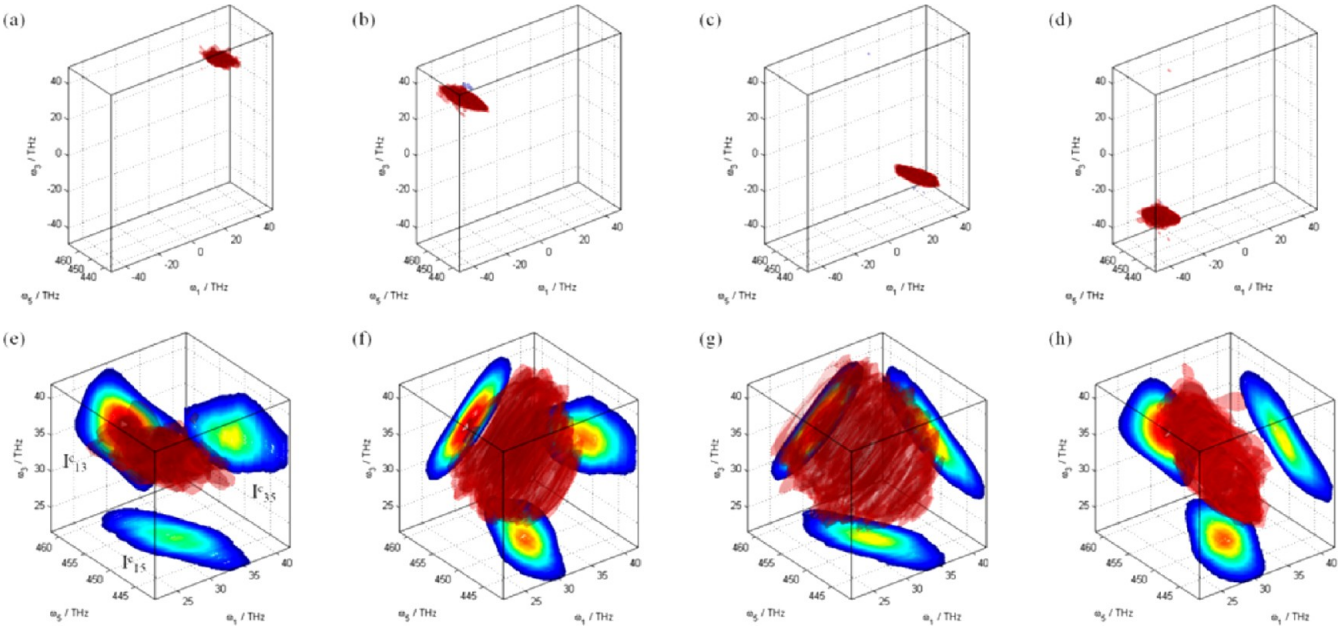

Figure 10. (a−d) Isosurfaces of 3D spectra from a 3 × 3 × 3 × 1 phase cycling scheme with causality imposed. The positions of the signals are the same as those in the causality imposed 2 × 2 × 2 × 1 phase cycling scheme. (e−h) Magnified view of the respective peaks and their 2D projections. All the 2D projections have phase-twisted features.

is by measuring the signal intensity with varying concentration. A fifth-order signal scales linearly with increasing concentration, while third-order cascades scale quadratically with concentration.[51] In Figure 12, the peak signal intensity of the 3D spectra shows a linear dependence on concentration, demonstrating that the majority of the signal from the experimental conditions presented here is from a fifth-order process rather than cascades.

dx.doi.org/10.1021/jp4046403 | J. Phys. Chem. B 2013, 117, 15369−15385

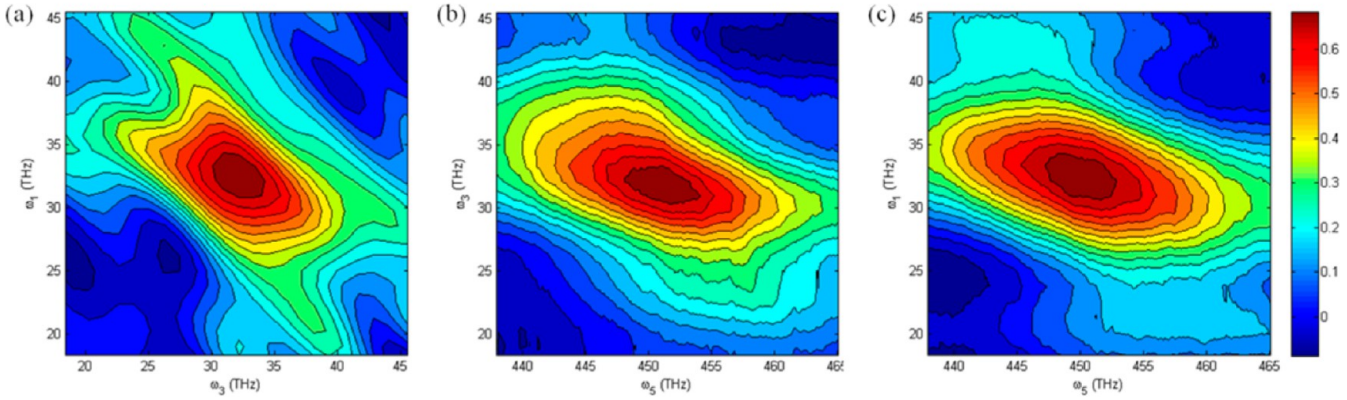

Figure 11. 2D projections of Figure 10e in a causality imposed 3 × 3 × 3 × 1 phase cycling scheme are shown. The projections (a) I^{c}_{13}, (b) I^{c}_{35}, and (c) I^{c}_{15} all show phase-twisted features, which is akin to a non-rephasing peak shape in a 2D spectrum.

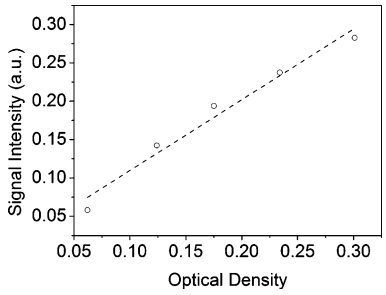

Figure 12. The maximum intensity of the measured pure absorptive signal is plotted against the optical density of the sample with various concentrations. A best fit line (dashed) is drawn. The heterodyned fifth-order signal should scale linearly with concentration c, while cascaded third-order signals should be linear with c^2. This shows that cascaded third-order signals do not contribute significantly to the 3D spectra.

Using a simple calculation,[9,10] together with the consideration of sample absorption, the cascading signal contributes ∼10% of the total signal at an optical density of 0.2. With optically thinner samples, the percentage contribution of cascades is further reduced.

VI. CONCLUDING REMARKS

We have presented the theoretical framework on how to obtain fifth-order 3D electronic spectroscopy using a pulse shaper assisted pump probe beam geometry. The use of the pulse shaper allows phase cycling to be performed that is able to selectively measure fifth-order signal. We discuss how purely absorptive 3D spectra as well as 3D spectra of processes from various coherence pathway processes can be obtained using phase cycling and data treatment. In the most general case, this requires a 27-step phase cycling scheme, but an 8-step phase cycling scheme may be adequate for a two-level system if the rotating frame reference frequency is chosen to be sufficiently far away from the resonance frequencies. There is only a small contribution of cascading third-order contribution to the fifth-order signals in this pump−probe geometry setup, as deduced by the linear relationship between the absorption intensity and sample concentration. The current demonstration is performed on a quasi-two-level system. We are currently working on understanding the applications of the phase cycling schemes and its restrictions for multilevel systems. In principle, the phase cycling scheme selection procedure demonstrated here in 3DES as well as in 2DES[23] can be applied to other nonlinear optical processes including extensions to even higher dimensional optical spectroscopy. It is hoped that this present article can spur further theoretical and numerical studies of fifth-order 3D spectroscopy and associated fifth-order optical processes[15,52,53] to complement the advancement in experimental techniques.

■ ASSOCIATED CONTENT

Supporting Information

Details on all the possible coherence pathways allowed in a pump−probe geometry and the expression of the 3 × 3 × 3 × 1 phase cycling scheme. This material is available free of charge via the Internet at http://pubs.acs.org.

■ AUTHOR INFORMATION

Corresponding Author

*E-mail: howesiang@ntu.edu.sg.

Notes

The authors declare no competing financial interest.

■ ACKNOWLEDGMENTS

This work is supported by the Singapore National Research Foundation (NRF-CRP5-2009-04) and the Singapore Agency for Science, Technology and Research Science and Engineering, (A*STAR SERC Grant No. 102-149-0153). Z.Z. thanks the Nanyang President's Graduate Scholarship for support. M.T.S. thanks the Lee Kuan Yew Postdoctoral Fellowship for financial support.

■ REFERENCES

(1) Jonas, D. M. Two-Dimensional Femtosecond Spectroscopy. *Annu. Rev. Phys. Chem.* **2003**, *54*, 425−463.
(2) Khalil, M.; Demirdöven, N.; Tokmakoff, A. Coherent 2D IR Spectroscopy: Molecular Structure and Dynamics in Solution. *J. Phys. Chem. A* **2003**, *107*, 5258−5279.
(3) Hochstrasser, R. M. Two-Dimensional Spectroscopy at Infrared and Optical Frequencies. *Proc. Natl. Acad. Sci. U.S.A.* **2007**, *104*, 14190−14196.
(4) Cho, M. Coherent Two-Dimensional Optical Spectroscopy. *Chem. Rev.* **2008**, *108*, 1331−1418.
(5) Mukamel, S.; Tanimura, Y.; Hamm, P. Coherent Multidimensional Optical Spectroscopy. *Acc. Chem. Res.* **2009**, *42*, 1207−1209.
(6) Hamm, P.; Zanni, M. T. *Concepts and Methods of 2D Infrared Spectroscopy*; Cambridge University Press: New York, 2011.

(7) Garrett-Roe, S.; Hamm, P. Purely Absorptive Three-Dimensional Infrared Spectroscopy. *J. Chem. Phys.* **2009**, *130*, 164510.
(8) Fidler, A. F.; Harel, E.; Engel, G. S. Dissecting Hidden Couplings Using Fifth-Order Three-Dimensional Electronic Spectroscopy. *J. Phys. Chem. Lett.* **2010**, *1*, 2876−2880.
(9) Garrett-Roe, S.; Perakis, F.; Rao, F.; Hamm, P. Three-Dimensional Infrared Spectroscopy of Isotope-Substituted Liquid Water Reveals Heterogeneous Dynamics. *J. Phys. Chem. B* **2011**, *115*, 6976−6984.
(10) Ding, F.; Fulmer, E. C.; Zanni, M. T. Heterodyned Fifth-Order Two-Dimensional IR Spectroscopy: Third-Quantum States and Polarization Selectivity. *J. Chem. Phys.* **2005**, *123*, 094502.
(11) Fulmer, E. C.; Ding, F.; Mukherjee, P.; Zanni, M. T. Vibrational Dynamics of Ions in Glass from Fifth-Order Two-Dimensional Infrared Spectroscopy. *Phys. Rev. Lett.* **2005**, *94*, 067402.
(12) Ding, F.; Zanni, M. T. Heterodyned 3D IR Spectroscopy. *Chem. Phys.* **2007**, *341*, 95−105.
(13) Schlau-Cohen, G. S.; Ishizaki, A.; Fleming, G. R. Two-Dimensional Electronic Spectroscopy and Photosynthesis: Fundamentals and Applications to Photosynthetic Light-Harvesting. *Chem. Phys.* **2011**, *386*, 1−22.
(14) Schlau-Cohen, G. S.; Calhoun, T. R.; Ginsberg, N. S.; Read, E. L.; Ballottari, M.; Bassi, R.; Van Grondelle, R.; Fleming, G. R. Pathways of Energy Flow in LHCII from Two-Dimensional Electronic Spectroscopy. *J. Phys. Chem. B* **2009**, *113*, 15352−15363.
(15) Hamm, P. Three-Dimensional-Ir Spectroscopy: Beyond the Two-Point Frequency Fluctuation Correlation Function. *J. Chem. Phys.* **2006**, *124*, 124506.
(16) Garrett-Roe, S.; Hamm, P. What Can We Learn from Three-Dimensional Infrared Spectroscopy? *Acc. Chem. Res.* **2009**, *42*, 1412−1422.
(17) Turner, D. B.; Stone, K. W.; Gundogdu, K.; Nelson, K. A. Three-Dimensional Electronic Spectroscopy of Excitons in GaAs Quantum Wells. *J. Chem. Phys.* **2009**, *131*, 144510.
(18) Davis, J. A.; Hall, C. R.; Dao, L. V.; Nugent, K. A.; Quiney, H. M.; Tan, H. H.; Jagadish, C. Three-Dimensional Electronic Spectroscopy of Excitons in Asymmetric Double Quantum Wells. *J. Chem. Phys.* **2011**, *135*, 044510.
(19) Li, H.; Bristow, A. D.; Siemens, M. E.; Moody, G.; Cundiff, S. T. Unraveling Quantum Pathways Using Optical 3D Fourier-Transform Spectroscopy. *Nat. Commun.* **2013**, *4*, 1390.
(20) DeFlores, L. P.; Nicodemus, R. A.; Tokmakoff, A. Two-Dimensional Fourier Transform Spectroscopy in the Pump-Probe Geometry. *Opt. Lett.* **2007**, *32*, 2966−2968.
(21) Myers, J. A.; Lewis, K. L. M.; Tekavec, P. F.; Ogilvie, J. P. Two-Color Two-Dimensional Fourier Transform Electronic Spectroscopy with a Pulse-Shaper. *Opt. Express* **2008**, *16*, 17420−17428.
(22) Shim, S. H.; Zanni, M. T. How to Turn Your Pump-Probe Instrument into a Multidimensional Spectrometer: 2D IR and Vis Spectroscopies via Pulse Shaping. *Phys. Chem. Chem. Phys.* **2009**, *11*, 748−761.
(23) Zhang, Z.; Wells, K. L.; Hyland, E. W. J.; Tan, H.-S. Phase-Cycling Schemes for Pump−Probe Beam Geometry Two-Dimensional Electronic Spectroscopy. *Chem. Phys. Lett.* **2012**, *550*, 156−161.
(24) Kumar, S. K. K.; Tamimi, A.; Fayer, M. D. Dynamics in the Interior of AOT Lamellae Investigated with Two-Dimensional Infrared Spectroscopy. *J. Am. Chem. Soc.* **2013**, *135*, 5118−5126.
(25) Zhang, Z.; Wells, K. L.; Tan, H. S. Purely Absorptive Fifth-Order Three-Dimensional Electronic Spectroscopy. *Opt. Lett.* **2012**, *37*, 5058−5060.
(26) Albrecht, A. W.; Hybl, J. D.; Gallagher Faeder, S. M.; Jonas, D. M. Experimental Distinction between Phase Shifts and Time Delays: Implications for Femtosecond Spectroscopy and Coherent Control of Chemical Reactions. *J. Chem. Phys.* **1999**, *111*, 10934−10956.
(27) Keusters, D.; Tan, H. S.; Warren, W. S. Role of Pulse Phase and Direction in Two-Dimensional Optical Spectroscopy. *J. Phys. Chem. A* **1999**, *103*, 10369−10380.
(28) Tian, P.; Keusters, D.; Suzaki, Y.; Warren, W. S. Femtosecond Phase-Coherent Two-Dimensional Spectroscopy. *Science* **2003**, *300*, 1553−1555.
(29) Tan, H.-S. Theory and Phase-Cycling Scheme Selection Principles of Collinear Phase Coherent Multi-Dimensional Optical Spectroscopy. *J. Chem. Phys.* **2008**, *129*, 124501.
(30) Yan, S.; Tan, H. S. Phase Cycling Schemes for Two-Dimensional Optical Spectroscopy with a Pump-Probe Beam Geometry. *Chem. Phys.* **2009**, *360*, 110−115.
(31) Monmayrant, A.; Weber, S.; Chatel, B. A Newcomer's Guide to Ultrashort Pulse Shaping and Characterization. *J. Phys. B: At., Mol. Opt. Phys.* **2010**, *43*.
(32) Schlau-Cohen, G. S.; Ishizaki, A.; Calhoun, T. R.; Ginsberg, N. S.; Ballottari, M.; Bassi, R.; Fleming, G. R. Elucidation of the Timescales and Origins of Quantum Electronic Coherence in Lhcii. *Nat. Chem.* **2012**, *4*, 389−395.
(33) Wong, C. Y.; Alvey, R. M.; Turner, D. B.; Wilk, K. E.; Bryant, D. A.; Curmi, P. M. G.; Silbey, R. J.; Scholes, G. D. Electronic Coherence Lineshapes Reveal Hidden Excitonic Correlations in Photosynthetic Light Harvesting. *Nat. Chem.* **2012**, *4*, 396−404.
(34) Mukamel, S. *Principles of Nonlinear Optical Spectroscopy*; Oxford University Press: New York, 1995.
(35) Seidner, L.; Stock, G.; Domcke, W. Nonperturbative Approach to Femtosecond Spectroscopy: General Theory and Application to Multidimensional Nonadiabatic Photoisomerization Processes. *J. Chem. Phys.* **1995**, *103*, 3998−4011.
(36) Kato, T.; Tanimura, Y. Multi-Dimensional Vibrational Spectroscopy Measured from Different Phase-Matching Conditions. *Chem. Phys. Lett.* **2001**, *341*, 329−337.
(37) Gelin, M. F.; Egorova, D.; Domcke, W. Efficient Calculation of Time- and Frequency-Resolved Four-Wave-Mixing Signals. *Acc. Chem. Res.* **2009**, *42*, 1290−1298.
(38) Cina, J. A. Wave-Packet Interferometry and Molecular State Reconstruction: Spectroscopic Adventures on the Left-Hand Side of the Schrödinger Equation. *Annu. Rev. Phys. Chem.* **2008**, *59*, 319−342.
(39) Lott, G. A.; Perdomo-Ortiz, A.; Utterback, J. K.; Widom, J. R.; Aspuru-Guzik, A.; Marcus, A. H. Conformation of Self-Assembled Porphyrin Dimers in Liposome Vesicles by Phase-Modulation 2D Fluorescence Spectroscopy. *Proc. Natl. Acad. Sci. U.S.A.* **2011**, *108*, 16521−16526.
(40) Perdomo-Ortiz, A.; Widom, J. R.; Lott, G. A.; Aspuru-Guzik, A.; Marcus, A. H. Conformation and Electronic Population Transfer in Membrane-Supported Self-Assembled Porphyrin Dimers by 2D Fluorescence Spectroscopy. *J. Phys. Chem. B* **2012**, *116*, 10757−10770.
(41) Tekavec, P. F.; Myers, J. A.; Lewis, K. L. M.; Ogilvie, J. P. Two-Dimensional Electronic Spectroscopy with a Continuum Probe. *Opt. Lett.* **2009**, *34*, 1390−1392.
(42) Tekavec, P. A.; Lewis, K. L. M.; Fuller, F. D.; Myers, J. A.; Ogilvie, J. P. Toward Broad Bandwidth 2-D Electronic Spectroscopy: Correction of Chirp from a Continuum Probe. *IEEE J. Sel. Top. Quantum Electron.* **2012**, *18*, 210−217.
(43) Keusters, D.; Warren, W. S. Effect of Pulse Propagation on the Two-Dimensional Photon Echo Spectrum of Multilevel Systems. *J. Chem. Phys.* **2003**, *119*, 4478−4489.
(44) Keusters, D.; Warren, W. S. Propagation Effects on the Peak Profile in Two-Dimensional Optical Photon Echo Spectroscopy. *Chem. Phys. Lett.* **2004**, *383*, 21−24.
(45) Yetzbacher, M. K.; Belabas, N.; Kitney, K. A.; Jonas, D. M. Propagation, Beam Geometry, and Detection Distortions of Peak Shapes in Two-Dimensional Fourier Transform Spectra. *J. Chem. Phys.* **2007**, *126*, 044511.
(46) Ernst, R. R.; Bodenhausen, G.; Wokaun, A. *Principles of Nuclear Magnetic Resonance in One and Two Dimensions*; Oxford University Press: New York, 1987.
(47) Wells, K. L.; Zhang, Z.; Rouxel, J. R.; Tan, H. S. Measuring the Spectral Diffusion of Chlorophyll a Using Two-Dimensional Electronic Spectroscopy. *J. Phys. Chem. B* **2012**, *117*, 2294−2299.
(48) Ulness, D. J.; Kirkwood, J. C.; Albrecht, A. C. Competitive Events in Fifth Order Time Resolved Coherent Raman Scattering:

Direct Versus Sequential Processes. *J. Chem. Phys.* **1998**, *108*, 3897−3902.
(49) Blank, D. A.; Kaufman, L. J.; Fleming, G. R. Fifth-Order Two-Dimensional Raman Spectra of Cs_2 Are Dominated by Third-Order Cascades. *J. Chem. Phys.* **1999**, *111*, 3105−3114.
(50) Kubarych, K. J.; Milne, C. J.; Miller, R. J. D. Fifth-Order Two-Dimensional Raman Spectroscopy: A New Direct Probe of the Liquid State. *Int. Rev. Phys. Chem.* **2003**, *22*, 497−532.
(51) Fulmer, E. C.; Ding, F.; Zanni, M. T. Heterodyned Fifth-Order 2D-IR Spectroscopy of the Azide Ion in an Ionic Glass. *J. Chem. Phys.* **2005**, *122*, 1−12.
(52) Okumura, K.; Tanimura, Y. The (2n+1)th-Order Off-Resonant Spectroscopy from the (n+1)th-Order Anharmonicities of Molecular Vibrational Modes in the Condensed Phase. *J. Chem. Phys.* **1997**, *106*, 1687−1698.
(53) Pakoulev, A. V.; Block, S. B.; Yurs, L. A.; Mathew, N. A.; Kornau, K. M.; Wright, J. C. Multiply Resonant Coherent Multidimensional Spectroscopy: Implications for Materials Science. *J. Phys. Chem. Lett.* **2010**, *1*, 822−828.